Structural, Electronic and Optical Properties of Double Perovskite Oxide Ca_2InAsO_6: A First Principles Approach

Course Title : Thesis
Course Code : TPG-599

Submitted by

Exam Roll : 106706
Registration Number : 2016214716
Academic Year : 2020-21
Session : 2016-17

This thesis is submitted to the Department of Theoretical Physics at University of Dhaka in partial fulfillment of the requirements for the degree of Masters of Science in Theoretical Physics.

July 4, 2023

Acknowledgement

At first, I would like to praise the almighty Allah, the most Gracious and the most Merciful, for the blessing on the completion of this thesis.

I would like to express my heartfelt gratitude to my supervisor, Dr. Mohammad Abdur Rashid, for his continuous supervision, insightful suggestions, and constant encouragement throughout the entire process of researching and writing this thesis. I am sincerely thankful to him for his technical support in shaping this work.

I am also grateful to the authors of many publications and books who indirectly helped me complete this work, as well as to the numerous scientific journals from which I got a lot of information for this work.

Abstract

The structural, electronic, and optical properties of Ca_2InAsO_6 double perovskite oxide are studied using the full potential linearized augmented plane wave (FP-LAPW) method based on density functional theory (DFT). The tolerance factor (τ) and the octahedral factor (μ) of about 0.84 and 0.45 are calculated, respectively, confirming that this compound forms a stable structure. Our calculations revealed that Ca_2InAsO_6 is a semiconductor with a moderate Γ point direct bandgap of about 2.83 eV, obtained with the modified Becke-Johnson level of theory. Furthermore, optical properties show interesting phenomena, as this material exhibits a good absorption coefficient in the visible region of the spectrum. The tunable moderate bandgap and good optical absorption in the visible light region suggest that the double perovskite material is suitable for use in different electronic and optical applications, especially in new energy production applications.

Contents

List of Figures

List of Tables

Chapter 1

Introduction

Over the course of time, the large scale consumption of energy and depletion of running energy sources at an alarming scale have inspired the scientific community to explore the new resources of renewable energy [1]. In the past decade, due to the variety of applications of double perovskite oxides, especially their great use in energy production devices, they have attracted great interest from both theoretical and experimental points of view. In recent years, double perovskite (DP) materials; have attracted much attention due to their promising applications in different fields, such as light-emitting diodes (LEDs), lasers, radiation detectors, and solar cells [2–6]. For clean energy, the Organic-inorganic based perovskites of ABX_3, where A is cations of the tetrahedral site (Cs^+, or CH_3NH_3), B is Pb metal at octahedral site, and X is halogen atoms, are outstanding materials which have fascinated substantial consideration in current years [7–9]. Their remarkable optical properties like a broad absorption band in the visible region, tunable bandgap, high mobility, low carrier effective masses, large photoconductivity, and lifetime with extended charge diffusion capability [10–12]. The materials become more fascinating for solar cells with the passage of time due to the sharpest increases in power conversion efficiency (PCE) which extends to 25.6% presently from 3.8% in 2009 [13, 14].

The tremendous progress in PCE of Pb containing organic-based perovskites enables them for optical and solar cells applications. However, challenges of instability render their commercialization because of toxicity of lead, temperature, and moisture/air. Therefore, the demand for nontoxic and stable makes the potential for advanced solar cells technology [15, 16]. The instability problem of organic-based

perovskite halides had been addressed by carbon encapsulation, integration of hydrophobic fractions, and multi-cation substitution. However, the toxicity due to Pb only is removed by its substitution with other elements. The best Pb substitute reside in the same group i.e., group-IVA germanium (Ge), and tin (Sn) [17,18]. However, it is noted that the Sn containing perovskites are reduces their stability as compared to Pb-based perovskites because of their fast deprivation in air. Furthermore, the substitution of Pb by Ge causes lessening of optical conductivity, light absorption, and dielectric constant which decreases the optical performance of devices [19]. Clearly, for the growth of the photovoltaic, and solar cells industry, the effective replacement of Pb is very significant. In recent years, the complex replacement of Pb has been incorporated by monovalent, and trivalent cations to explore the new derivate of perovskite known as DPs. These have the formula $A_2B'B''X_6$, in that symbol A denotes a large cation similar to Cs^+ whereas, B' and B'' are reffered as monovalent and trivalent cations, and X is halides or oxygen. Presently, DPs have become promising for photovoltaic, and solar cells [20]. It is anticipated that analysis of several arrangements of B' and B'' can create prospects to find suitable high-efficiency Pb-free DPs. In DPs the possible options of B' site like K^+, Rb^+, Ag^+, In^+, Au^+, and B'' site like Sb^{3+}, Bi^{3+}, etc. [21]. In literature, the synthetic protocol and remarkable characterization and electro-optical characteristics have already been explored for several inorganic DPs oxides. Brik et at., investigated the electronic structure and optical characteristics of Ba_2MgWO_6. The bandgap of 2.48 eV and absorption in the ultraviolet region [22]. Later on many DPs are explored and characterized for different applications like Ba_2HoReO_6 for magnetic properties [23], Ba_2SmNbO_6 and Ba_2ZnOsO_6 for magnetic, thermodynamic, and thermoelectric [24, 25], doping effect of Ba on transport behavior of Sr_2TiMoO_6 [26,27], A_2FeReO_6 (A = Sr, Ba) is illustrated for 5d electrons effect on optical properties [28], and electronic behavior of Ba_2CdOsO_6 . Moreover, Thind et al. investigated experimentally: $KBaTeBiO_6$ and found a bandgap of 1.88 eV which makes it promising for solar cells.

This thesis has been arranged into six chapters, starting with the introductory chapter. In Chapter 2, the schrödinger equation is discussed for charged particles and is extended to the development of a generalized many-body schrödinger equation for a system made up of electrons and nuclei where external magnetic and electric fields are neglected. At the end of this chapter, The Hatree-Fock method, a traditional approach, is discussed, which is used to find approximate solutions of the

wave function and the energy of a quantum many-body system in a stationary state. In Chapter 3, an advanced theoretical approach, Density Functional Theory, is discussed, which provides a way to systematically map the many-body problem with electron-electron interaction energy onto a single-body problem without electron-electron interaction energy. At the end of this chapter, some approximations have been discussed to determine the exact functionals for exchange and correlation. In chapter 4, the details of the calculations are discussed thoroughly. In Chapter 5, the structural, electronic, and optical properties have been discussed in detail, and finally, in Chapter 6, all the results of the study are summarized.

Chapter 2

Basic Quantum Mechanics

Quantum mechanics is a branch of physics that describes the behaviour of matter and energy at the smallest scales, such as atoms and subatomic particles, although there are also certain macroscopic systems it directly applies to. This chapter goes through basic concepts and expressions, as well as the most basic forms that are applicable to many-body systems. In quantum physics, particles have wavelike properties, and a particular wave equation, the Schrödinger equation, governs how these waves behave. The Schrödinger equation is different in a few ways from the other wave equations. But these differences won't keep us from applying all of our usual strategies for solving a wave equation and dealing with the resulting solutions.

2.1 The Schrödinger Equation

The principle of density functional theory are conveniently expounded by making reference to conventional wave function theory. Any problem in the electronic structure of matter is covered by Schrödinger's equation [29]. In 1926, Erwin Schrödinger attempted to characterize matter waves by using de Broglie's connections to describe hypothetical plane waves, resulting in the most generic form of the famous equation named after him, the time-dependent Schrödinger equation [30]

$$i\hbar\frac{\partial}{\partial t} = \hat{H}\psi(\vec{r},t) \tag{2.1}$$

Where, $\hat{H}$ is the hamiltonian operator, $\hbar$ is the dirac constant and ψ is the wave function. It is often impracticable to use a complete relativistic formulation of the formula; therefore Schrödinger himself postulated a non-relativistic approximation which is nowadays often used, especially in quantum chemistry. Using the Hamiltonian for a single particle

$$\hat{H} = \hat{T} + \hat{V} = -\frac{\hbar^2}{2m}\vec{\nabla}^2 + V(\vec{r}, t) \tag{2.2}$$

leads to the (non-relativistic) time-dependent single-particle Schrödinger equation

$$i\hbar\frac{\partial}{\partial t}\psi(\vec{r}, t) = [-\frac{\hbar^2}{2m}\vec{\nabla}^2 + V(\vec{r}, t)]\psi(\vec{r}, t) \tag{2.3}$$

The Hamiltonian for N particles in three dimensions is

$$\hat{H} = \sum_{i=1}^{N}\frac{\hat{p}_i^2}{2m_i} + V(\vec{r}_1, \vec{r}_2, \ldots \vec{r}_N, t) = -\frac{\hbar^2}{2}\sum_{i=1}^{N}\frac{1}{m_i} + V(\vec{r}_1, \vec{r}_2, \ldots \vec{r}_N, t) \tag{2.4}$$

The corresponding Schrödinger equation reads

$$i\hbar\frac{\partial}{\partial t}\psi(\vec{r}_1, \vec{r}_2, \ldots \vec{r}_N, t) = [-\frac{\hbar^2}{2}\sum_{i=1}^{N}\frac{1}{m_i}\nabla_i^2 + V(\vec{r}_1, \vec{r}_2, \ldots \vec{r}_N, t)]\psi(\vec{r}_1, \vec{r}_2, \ldots \vec{r}_N, t) \tag{2.5}$$

2.2 Time-independent Schrödinger Equation

Special cases are the solutions of the time-independent Schrödinger equation, where the Hamiltonian itself has no time-dependency (which implies a time-independent potential V $(\vec{r}_1, \vec{r}_2, \ldots \vec{r}_N)$ and the solutions therefore describe standing waves which are called stationary states or orbitals). The time-independent Schrödinger equation is not only easier to treat, but the knowledge of its solutions also provides crucial

insight to handle the corresponding time-dependent equation. The time-independent equation (2.5) is obtained by the approach of separation of variables, i.e. the spatial part of the wave function is separated from the temporal part via [31].

$$\Psi(\vec{r}_1, \vec{r}_2, \ldots \vec{r}_N, t) = \psi(\vec{r}_1, \vec{r}_2, \ldots \vec{r}_N)\tau(t) = \psi(\vec{r}_1, \vec{r}_2, \ldots \vec{r}_N)e^{\frac{iEt}{\hbar}} \tag{2.6}$$

Furthermore, the l.h.s. of the equation reduces to the energy eigenvalue of the Hamiltonian multiplied by the wave function, leading to the general eigenvalue equation

$$E\psi(\vec{r}_1, \vec{r}_2, \ldots \vec{r}_N) = \hat{H}\psi(\vec{r}_1, \vec{r}_2, \ldots \vec{r}_N) \tag{2.7}$$

Again, using the many-body Hamiltonian, the Schrödinger equation becomes

$$E\psi(\vec{r}_1, \vec{r}_2, \ldots \vec{r}_N) = [-\frac{\hbar^2}{2}\sum_{i=1}^{N}\frac{1}{m_i}\nabla_i^2 + V(\vec{r}_1, \vec{r}_2, \ldots \vec{r}_N)]\psi(\vec{r}_1, \vec{r}_2, \ldots \vec{r}_N) \tag{2.8}$$

2.3 The Many-Body System and Born-Oppenheimer (BO) Approximation

Charged particles are present in all atomic and molecular systems. The Schrödinger equation for a single electron, in which the electron moves in a Coulomb potential

$$i\hbar\frac{\partial}{\partial t}\psi(\vec{r}) = \left[-\frac{\hbar^2}{2m}\vec{\nabla}^2 - \frac{e^2}{4\pi\epsilon_o}\frac{1}{|\vec{r}|}\right]\psi(\vec{r}) \tag{2.9}$$

The so-called atomic units are introduced at this stage for future use for the purpose of simplicity. That is, the electron mass m_e, the electron charge e, the reduced Planck constant (Dirac constant), $\hbar$ and the vacuum permittivity factor $4\pi\epsilon_o$ are all equal to one [32]. The Schrödinger equation for the single electron simplifies

to

$$E\psi(\vec{r}) = \left[-\frac{1}{2}\vec{\nabla}^2 - \frac{1}{|\vec{r}|}\right]\psi(\vec{r}) \tag{2.10}$$

The Schrödinger equation can be solved analytically in this way. Although the Schrödinger equation will soon be analytically accessible for the description of matter, including atoms. The use of (2.8) allows the development of a generalized many-body Schrödinger equation for a system made up of N electrons and M nuclei, where external magnetic and electric fields are neglected.

$$E_i\psi_i(\vec{r}_1\vec{r}_2\ldots\vec{r}_N;\vec{R}_1\vec{R}_2\ldots\vec{R}_N) = \hat{H}\psi(\vec{r}_1\vec{r}_2\ldots\vec{r}_N;\vec{R}_1\vec{R}_2\ldots\vec{R}_N) \tag{2.11}$$

Equation (2.11) does not seem overly complicated on the first look, but an examination of the corresponding molecular Hamiltonian

$$\hat{H} = -\frac{\hbar^2}{2m_e}\sum_{i=1}^{N}\nabla_i^2 - \frac{\hbar^2}{2M_k}\sum_{k=1}^{M}\nabla_k^2 - \sum_{i=1}^{N}\sum_{k=1}^{M}\frac{Z_k e^2}{r_{ik}} + \frac{1}{2}\sum_{i=1}^{N}\sum_{j>i}^{N}\frac{e^2}{r_{ij}} + \frac{1}{2}\sum_{k=1}^{M}\sum_{l>k}^{M}\frac{Z_k Z_l}{R_{kl}} \tag{2.12}$$

reveals the real complexity of the equation. In equation (2.12), M_k represents the nuclear mass in atomic units (i.e. in units of the electron mass), Z_k and Z_l represent the atomic numbers, and $\vec{r}_{ij} = |\vec{r}_i - \vec{r}_j|$, $\vec{r}_{ik} = |\vec{r}_i - \vec{r}_k|$, $\vec{R}_{kl} = |\vec{R}_k - \vec{R}_l|$ represent the distances between electron-electron, electron-nucleus and nucleus-nucleus respectively. A term-by-term interpretation of the right hand side in (2.12) reveals that the first two terms correspond to the kinetic energies of the electrons and nuclei. The latter three terms denote the potential part of the Hamiltonian in terms of electrostatic particle-particle interactions. This is reflected by the corresponding signs, where the negative sign denotes an attractive potential between electrons and nuclei, whereas the positive signs denote repulsive potentials between electrons and electrons as well as the nuclei among themselves [33].

The Born-Oppenheimer approximation is one of the basic concepts underlying the description of the quantum states of molecules. This approximation makes it possible to separate the motion of the nuclei and the motion of the electrons. In this discussion nuclear refers to the atomic nuclei as parts of molecules not to the internal structure of the nucleus. The Born-Oppenheimer approximation neglects the motion of the atomic nuclei when describing the electrons in a molecule. The physical basis for the Born-Oppenheimer approximation is the fact that the mass of an atomic nucleus in a molecule is much larger than the mass of an electron (more than 1000 times). Because of this difference, the nuclei move much more slowly than the electrons. In addition, due to their opposite charges, there is a mutual attractive force of acting on an atomic nucleus and an electron. This force causes both particles to be accelerated. Since the magnitude of the acceleration is inversely proportional to the mass. The acceleration of the electrons is large and the acceleration of the atomic nuclei is small; the difference is a factor of more than 1000. As a consequence, the general Hamiltonian is replaced by the so-called electronic Hamiltonian from equation (2.12)

$$\hat{H} = -\frac{\hbar^2}{2m_e}\sum_{i=1}^{N}\nabla_i^2 - \sum_{i=1}^{N}\sum_{k=1}^{M}\frac{Z_k e^2}{r_{ik}} + \frac{1}{2}\sum_{i=1}^{N}\sum_{j>i}^{N}\frac{e^2}{r_{ij}} \tag{2.13}$$

or in terms of operators

$$\hat{H}_{el} = \hat{T} + \hat{U} + \hat{V} = \hat{T} + \hat{V}_{tot} \tag{2.14}$$

Especially for problems of molecular physics and quantum chemistry, the electronic Schrödinger equation is of major interest. But despite all simplifications a simple look at equations (2.11) to (2.14) indicates that there are still a few more crucial points left to deal with until a useful solution can be obtained. Inspection of equations (2.13) and (2.14) shows that the kinetic energy term $\hat{T}$ doesn't depend on the nuclear coordinates R_{kl}, or in other words, it is only a function of the electron number. Also the electron-electron repulsion $\hat{U}$ is the same for every system with only Coulomb interactions. Therefore the only part of the electronic Hamiltonian which depends

on the atomic molecular system is the external potential $\hat{V}$ caused by the nucleus-electron interaction. Subsequently this also means that $\hat{T}$ and $\hat{U}$ only need the electron number N as input and will therefore be denoted as 'universal', whereas $\hat{V}$ is system-dependent. The expectation value of $\hat{V}$ is also often denoted as the external potential V_{ext}, which is consistent as long as there are no external magnetic or electrical fields [34]. As soon as the external potential is known, the next step is the determination of the wave functions Ψ_i which contain all possible information about the system. As simple as that sounds, the exact knowledge of the external potential is not possible for most natural systems, i.e. in similarity to classical mechanics, the largest system which can be solved analytically is a two body system, which corresponds to a hydrogen atom. Using all approximations introduced up to now it is possible to calculate a problem similar to H_2^+, a single ionized hydrogen molecule. To get results for larger systems, further approximations have to be made.

2.4 Slater Determinant

A Slater determinant is an expression that describes the wave function of a multi-fermionic system. It satisfies anti-symmetry requirements, and consequently the Pauli principle, by changing sign upon exchange of two electrons (or other fermions) [35]. Only a small subset of all possible fermionic wave functions can be written as a single Slater determinant, but those form an important and useful subset because of their simplicity. In the Hartree-Fock approach, the search is restricted to approximations of the N-electron wave function by an antisymmetric product of N (normalized) one electron wave-functions, the so called spin-orbitals $\chi_i(\vec{x}_i)$. A wave function of this type is called Slater-determinant, and reads [36, 37].

$$\psi_o \approx \phi_{SD} = (N!)^{-\frac{1}{2}} \begin{vmatrix} \chi_1(\vec{x}_1) & \chi_2(\vec{x}_1) & \dots & \chi_N(\vec{x}_1) \\ \chi_1(\vec{x}_2) & \chi_2(\vec{x}_2) & \dots & \chi_N(\vec{x}_2) \\ \vdots & \vdots & \ddots & \vdots \\ \chi_1(\vec{x}_N) & \chi_2(\vec{x}_N) & \dots & \chi_N(\vec{x}_N) \end{vmatrix} \tag{2.15}$$

It is important to notice that the spin-orbitals $\chi_i(\vec{x}_i)$ are not only depending on spatial coordinates but also on a spin coordinate which is introduced by a spin

function, $\vec{x}_i = \vec{r}_i$, s. A detailed discussions of the spin orbitals and their (necessary) properties is provided in the books by Szabo and Holthausen [37].

2.5 The Hartree-Fock Method

The Hartree–Fock method is a method of approximation for the determination of the wave function and the energy of a quantum many-body system in a stationary state.In the following sections we set $\hat{H} \equiv \hat{H}_{el}$, $E \equiv E_{el}$, and so on. Observables in quantum mechanics are calculated as the expectation values of operators [31, 38]. The energy as observable corresponds to the Hamilton operator, therefore the energy corresponding to a general Hamiltonian can be calculated as

$$E = \langle \hat{H} \rangle = \int d\vec{r}_1 \int d\vec{r}_2 \ldots \int d\vec{r}_N \psi^*(\vec{r}_1, \vec{r}_2, \ldots, \vec{r}_N) \hat{H} \psi(\vec{r}_1, \vec{r}_2, \ldots, \vec{r}_N) \qquad (2.16)$$

The Hartree-Fock technique is based on the principle that the energy obtained by any (normalized) trial wave function other than the actual ground state wave function is always an upper bound, i.e. higher than the actual ground state energy. If the trial function happens to be the desired ground state wave function, the energies are equal

$$E_{trial} \geq E_o \qquad (2.17)$$

with

$$E_{trial} = \int d\vec{r}_1 \int d\vec{r}_2 \ldots \int d\vec{r}_N \psi^*_{trial}(\vec{r}_1, \vec{r}_2, \ldots, \vec{r}_N) \hat{H} \psi_{trial}(\vec{r}_1, \vec{r}_2, \ldots, \vec{r}_N) \qquad (2.18)$$

and

$$E_o = \int d\vec{r}_1 \int d\vec{r}_2 \ldots \int d\vec{r}_N \psi_o^*(\vec{r}_1, \vec{r}_2, \ldots, \vec{r}_N) \hat{H} \psi_o(\vec{r}_1, \vec{r}_2, \ldots, \vec{r}_N) \tag{2.19}$$

The expressions above are usually inconvenient to handle. For the sake of a compact notation, in the following the bracket notation of Dirac is introduced. For a detailed description of this notation, the reader is referred to the original publication [39]. In that notation, equations (2.17) to (2.19) are expressed as

$$\langle \psi_{trial} | \hat{H} | \psi_{trial} \rangle = E_{trial} \geq E_o = \langle \psi_o | \hat{H} | \psi_o \rangle \tag{2.20}$$

Proof: [38] The eigenfunctions ψ_i of the Hamiltonian $\hat{H}$ (each corresponding to an energy eigenvalue E_i form a complete basis set, therefore any normalized trial wave function ψ_{trial} can be expressed as linear combination of those eigen functions.

$$\psi_{trial} = \sum_i \lambda_i \psi_i \tag{2.21}$$

The assumption is made that the eigen functions are orthogonal and normalized. Hence it is requested that the trial wave function is normalized, it follows that

$$\langle \psi_{trial} | \psi_{trial} \rangle = 1 = \langle \sum_i \lambda_i \psi_i | \sum_j \lambda_j \psi_j \rangle = \sum_i \sum_j \lambda_i^* \lambda_j \langle \psi_i | \psi_j \rangle = \sum_j |\lambda_j|^2 \tag{2.22}$$

On the other hand, following (2.21) and (2.23)

$$E_{trial} = \langle \psi_{trial} | \hat{H} | \psi_{trial} \rangle = \langle \sum_i \lambda_i \psi_i | \hat{H} | \sum_j \lambda_j \psi_j \rangle = \sum_j E_j |\lambda_j|^2 \tag{2.23}$$

Together with the fact that the ground state energy E_o is per definition the lowest possible energy, and therefore has the smallest eigenvalue ($E_o \leq E_i$), it is found that

$$E_{trial} = \sum_j E_j |\lambda_j|^2 \geq E_o \sum_j |\lambda_j|^2 \tag{2.24}$$

what resembles equation (2.20). Equations (2.16) to (2.24) also include that a search for the minimal energy value while applied on all allowed N-electron wave-functions will always provide the ground-state wave function (or wave functions, in case of a degenerate ground state where more than one wave function provides the minimum energy). The mathematical framework used above, i.e.rules which assign numerical values to functions, so called functionals, is also one of the main concepts in density functional theory. A function gets a numerical input and generates a numerical output whereas a functional gets a function as input and generates a numerical output [40]. Expressed in terms of functional calculus, where $\psi \to N$ addresses all allowed N-electron wave functions, this means [37]

$$E_o = \underset{\psi \to N}{min}\, E[\psi] = \underset{\psi \to N}{min} \langle \psi | \hat{H} | \psi \rangle = \underset{\psi \to N}{min} \langle \psi | \hat{T} + \hat{V} + \hat{U} | \psi \rangle \tag{2.25}$$

For N-electron systems this search is, due to the large number of possible wave functions on the one hand and limitations in computational power and time, practically impossible. What is possible is the restriction of the search to a smaller subset of possible wave function, as it is done in the Hartree-Fock approximation. From equation (2.24), the ground state energy approximated by a single slater determinant becomes

$$E_o = \underset{\phi_{SD} \to N}{min}\, E[\phi] = \underset{\phi_{SD} \to N}{min} \langle \phi_{SD} | \hat{H} | \phi_{SD} \rangle = \underset{\phi_{SD} \to N}{min} \langle \phi_{SD} | \hat{T} + \hat{V} + \hat{U} | \phi_{SD} \rangle \tag{2.26}$$

A general expression for the Hartree-Fock Energy is obtained by usage of the Slater determinant as a trial function

$$E_{HF} = \langle \phi_{SD} | \hat{H} | \phi_{SD} \rangle = \langle \phi_{SD} | \hat{T} + \hat{V} + \hat{U} | \phi_{SD} \rangle \tag{2.27}$$

For the sake of brevity, a detailed derivation of the final expression for the Hartree-Fock energy is omitted. It is a straightforward calculation found for example in the Book by Schwabl [31]. The final expression for the Hartree- Fock energy contains three major parts [37]

$$E_{HF} = \langle \phi_{SD} | \hat{H} | \phi_{SD} \rangle = \sum_{i}^{N} (i|\hat{h}|i) + \frac{1}{2} \sum_{i}^{N} \sum_{j}^{N} [(ii|jj) - (ij|ji)] \tag{2.28}$$

$$(i|\hat{h}_i|i) = \int \chi_i^*(\vec{x}_i) \left[-\frac{1}{2} \vec{\nabla}_i^2 - \sum_{k=1}^{M} \frac{Z_k}{r_{ik}} \right] \chi_i(\vec{x}_i) d\vec{x}_i \tag{2.29}$$

$$(ii|jj) = \int \int |\chi_i(\vec{x}_i)|^2 \frac{1}{r_{ij}} |\chi_j(\vec{x}_j)|^2 d\vec{x}_i d\vec{x}_j \tag{2.30}$$

$$(ii|jj) = \int \int \chi_i(\vec{x}_i) \chi_j^*(\vec{x}_j) \frac{1}{r_{ij}} \chi_j(\vec{x}_j) \chi_i^*(\vec{x}_i) d\vec{x}_i d\vec{x}_j \tag{2.31}$$

The first term corresponds to the kinetic energy and the nucleus-electron interactions, $\hat{H}$ denoting the single particle contribution of the Hamiltonian,whereas the latter two terms correspond to electron-electron interactions. They are called Coulomb and exchange integral, respectively [36,37]. Examination of equations (2.28) to (2.31) furthermore reveals, that the Hartree-Fock energy can be expressed as a functional of the spin orbitals $E_{HF} = E[\{\chi_i\}]$. Thus,variation of the spin orbitals leads to the minimum energy [37]. An important point is that the spin orbitals remain orthonormal during minimization. This restriction is accomplished by the introduction of Lagrangian multipliers λ_i in the resulting equations, which represent the Hartree-Fock equations. For a detailed derivation, the reader is referred to the book by Szabo and Ostlund [36].

Finally, one arrives at

$$\hat{f} \chi_i = \lambda_i \chi_i \qquad i = 1, 2, \ldots, N \tag{2.32}$$

with

$$\hat{f}_i = -\frac{1}{2}\vec{\nabla}_i^2 - \sum_{k=1}^{M}\frac{Z_k}{r_{ik}} + \sum_{i}^{N}[\hat{J}_j(\vec{x}_i) - \hat{K}_j(\vec{x}_i)] = \hat{h}_i + \hat{V}^{HF}(i) \tag{2.33}$$

the Fock operator for the i-th electron. In similarity to(2.28) to (2.31), the first two terms represent the kinetic and potential energy due to nucleus-electron interaction, collected in the core Hamiltonian $\hat{h}_i$, whereas the latter terms are sums over the Coulomb operators $\hat{J}_j$ and the exchange operators $\hat{K}_j$ with the other j electrons, which form the Hartree-Fock potential $\hat{V}^{HF}$. There the major approximation of Hartree-Fock can be seen. The two electron repulsion operator from the original Hamiltonian is exchanged by a one electron operator $\hat{V}^{HF}$ which describes the repulsion in average. [37]

2.6 Limitations of the Hartree-Fock Method

The number of electrons in an atom or a molecule might be even or odd. The compound is in a singlet state if the number of electrons is even and they are all in double occupied spatial orbitals, ϕ_i. Closed-shell systems are what they are called. Open-shell systems are compounds with an odd number of electrons and compounds with single occupied orbitals, i.e. species with a triplet or higher ground state. These two sorts of systems relate to two different Hartree-Fock techniques. The restricted HF technique (RHF) considers all electrons to be coupled in orbitals, whereas the unconstrained HF method (UHF) removes this restriction entirely. Open-shell systems may alternatively be described using an RHF method, in which only the single occupied orbitals are eliminated, resulting in a limited open-shell HF (ROHF), which is more realistic but also more difficult and hence less popular than UHF [37]. Closed-shell systems, on the other hand, need an unlimited approach to get good outcomes. For example, a system that places both electrons in the same spatial orbital cannot properly describe the dissociation of H_2 (i.e. the behavior at high internuclear distances), because one electron must be positioned at one hydrogen atom. As a result, in HF calculations, technique selection is always crucial [41]. Kohn states several $M = P^5$ with $3 \leq p \leq 10$ parameters for an output with adequate accuracy in the investigations of the H_2 system [41]. For a system with N = 100 electrons, the number of

parameters rises to

$$M = p^{3N} = 3^{300} to 10^{300} \approx 10^{150} to 10^{300} \tag{2.34}$$

Equation (2.34) states, that the minimization of the energy would have to be performed in a space of at least 10^{150} dimension which exceeds the computational possibilities nowadays by far. HF-methods are therefore restricted to systems with a small number of involved electrons (N $\approx$ 10). Referring to the exponential factor in (2.34) this limitation is sometimes called exponential wall [41]. Since a many electron wave function cannot be described entirely by a single Slater determinant, the energy obtained by HF calculations is always larger than the exact ground state energy. The most accurate energy obtainable by HF-methods is called the Hartree-Fock-limit [37].

The difference between E_{HF} and E_{exact} is called correlation energy and can be denoted as [42]

$$E_{corr}^{HF} = E_{min} - E_{HF} \tag{2.35}$$

Despite the fact that E_{corr} is usually small against E_{min}, as in the example of a N_2 molecule where

$$E_{corr}^{HF} = 14.9eV < 0.001 E_{min} \tag{2.36}$$

it can have a huge in influence [43]. For instance, the experimental dissociation energy of the N_2 molecule is

$$E_{diss} = 9.9eV < E_{corr} \tag{2.37}$$

which corresponds to a large contribution of the correlation energy to relative

energies such as reaction energies which are of particular interest in quantum chemistry [43].

The main contribution to the correlation energy arises from the mean field approximation used in the HF-method. That means one electron moves in the average field of the other ones, an approach which completely neglects the intrinsic correlation of the electron movements. To get a better understanding what that means, one may picture the repulsion of electrons at small distances which clearly cannot be covered by a mean-field approach like the Hartree-Fock method [37].

Chapter 3

Density Functional Theory (DFT)

Density-functional theory (DFT) is a successful theory to calculate the electronic structure of atoms, molecules, and solids. Its goal is the quantitative understanding of material properties from the fundamental laws of quantum mechanics. Traditional electronic structure methods attempt to find approximate solutions to the Schrödinger equation of N interacting electrons moving in an external, electrostatic potential. However, there are serious limitations of this approach: (1) the problem is highly nontrivial, even for very small numbers N and the resulting wave functions are complicated objects and (2) the computational effort grows very rapidly with increasing N, so the description of larger systems becomes prohibitive. A different approach is taken in density-functional theory where, instead of the many-body wave function, the one-body density is used as the fundamental variable. Since the density n(r) is a function of only three spatial coordinates (rather than the 3N coordinates of the wave function), density-functional theory is computationally feasible even for large systems. The foundations of density-functional theory are the Hohenberg–Kohn and Kohn–Sham theorems which will be reviewed in the following section. In the section "The Exchange-Correlation Functionals," various levels of approximation to the central quantity of DFT are discussed.

3.1 The Electron Density

The electron density (for N electrons) as the basic variable of density functional theory is defined as [37, 44]

$$n(\vec{r}) = N \sum_{s_1} \int d\vec{x_2} \ldots \int d\vec{x}_N \psi^*(\vec{x}_1, \vec{x}_2, \ldots, \vec{x}_N) \psi^(\vec{x}_1, \vec{x}_2, \ldots, \vec{x}_N) \tag{3.1}$$

What has to be mentioned is that the notation in (3.1) considers a wave function dependent on spin and spatial coordinates. In detail, the integral in the equation gives the probability that a particular electron with arbitrary spin is found in the volume element $d\vec{r}_1$. Due to the fact that the electrons are indistinguishable, N times the integral gives the probability that any electron is found there. The other electrons represented by the wave function $\psi(\vec{x}_1, \vec{x}_2, \ldots, \vec{x}_N)$ have arbitrary spin and spatial coordinates [37].

If additionally the spin coordinates are neglected, the electron density can even be expressed as measurable observable only dependent on spatial coordinates [41, 44]

$$n(\vec{r}) = N \int d\vec{r_2} \ldots \int d\vec{r}_N \psi^*(\vec{r}_1, \vec{r}_2, \ldots, \vec{r}_N) \psi^(\vec{r}_1, \vec{r}_2, \ldots, \vec{r}_N) \tag{3.2}$$

which can e.g. be measured by X-ray diffraction [37].

Before presenting an approach using the electron density as variable, it has to be ensured that it truly contains all necessary informations about the system. In detail that means it has to contain information about the electron number N as well as the external potential characterized by $\hat{V}$ [37]. The total number of electrons can be obtained by integration the electron density over the spatial variables [37].

$$N = \int d\vec{r} n(\vec{r}) \tag{3.3}$$

3.2 The Thomas-Fermi Model

Density functional for the total internal electronic energy F[n] is to see if it can be constructed from basic physics ideas. Early attempts to create such an approximation were made by Thomas and Fermi [45–48]. They used some assumptions about the

distribution and the interaction between electrons to approximate the kinetic energy. The electron density in each space point is set equal to a number of electrons in a fixed volume, $n(r) = \frac{\Delta N}{\Delta V}$. A system of ΔN free non-interacting electrons in an infinite-well model of volume ΔV then gives an expression for the kinetic energy per volume. The continuity limit is then taken, $\Delta V \to 0$. The result is integrated over the whole space to give the approximate Thomas–Fermi functional for the total kinetic energy $T_{TF}[n]$,

$$T \approx T_{TF}[n] = \frac{3}{5}(3\pi^2)^{2/3}\left(\frac{\hbar^2}{2m_e}\right)\int n^{5/3}(\mathbf{r})d\mathbf{r} \tag{3.4}$$

Furthermore, the electrostatic energy of a classical repulsive gas $J[n]$ can be used as a simplistic approximation of the internal potential energy U,

$$U \approx J[n] = \frac{1}{2}\left(\frac{e_c^2}{4\pi\epsilon_o}\right)\int\int \frac{n(\mathbf{r}_1)n(\mathbf{r}_2)}{|\mathbf{r}_1 - \mathbf{r}_2|}d\mathbf{r}_1 d\mathbf{r}_2 \tag{3.5}$$

The result is the Thomas–Fermi model:

$$E_e \approx T_{TF}[n] + J[n] + \int n(\mathbf{r})v(\mathbf{r})d\mathbf{r} \tag{3.6}$$

The Thomas–Fermi approximation to the internal electronic energy thus is

$$F[n] \approx T_{TF}[n] + J[n] \tag{3.7}$$

3.3 The Hohenberg-Kohn (HK) Theorems

3.3.1 Theorem I

It states that the external potential $V(\vec{r})$ is a functional of the electrons density $n(\vec{r})$ and, up to an unimportant constant, uniquely determined by it. It is assumed that there exist two external potential $V(\vec{r})$ and $V^{'}(\vec{r})$ which differ by more than just a trivial constant. Furthermore the assumption is made, that both potentials give rise to the same electron density $n(\vec{r})$. Clearly arising from the nature of $\vec{V}$ in that case there have to be two different Hamiltonians $\hat{H}$ and $\hat{H}^{'}$. Furthermore Ψ and $\Psi^{'}$ have to be different Schrödinger equations. Finally also the energy $\hat{E}$ and $\hat{E}^{'}$ associated with the particular wave function differ. Now the two wave functions Ψ and $\Psi^{'}$ are used as trial functions assuming the other wave function is the ground state wave function. Then the expressions

$$E_o^{'} = \langle\psi^{'}|\hat{H}^{'}|\psi^{'}\rangle < \langle\psi|\hat{H}^{'}|\psi\rangle = \langle\psi|\hat{H}+\hat{V}^{'}-\hat{V}|\psi\rangle = \langle\psi|\hat{H}|\psi\rangle + \langle\psi|\hat{V}^{'}-\hat{V}|\psi\rangle \tag{3.8}$$

and

$$E_o = \langle\psi|\hat{H}|\psi\rangle < \langle\psi^{'}|\hat{H}|\psi^{'}\rangle = \langle\psi^{'}|\hat{H}^{'}+\hat{V}-\hat{V}^{'}|\psi^{'}\rangle = \langle\psi^{'}|\hat{H}^{'}|\psi^{'}\rangle + \langle\psi^{'}|\hat{V}-\hat{V}^{'}|\psi^{'}\rangle \tag{3.9}$$

are obtained. This can be rewritten as

$$E_o^{'} < E_o + \int [v^{'}(\vec{r}) - v(\vec{r})]n(\vec{r})d\vec{r} \tag{3.10}$$

$$E_o < E_o^{'} + \int [v(\vec{r}) - v^{'}(\vec{r})]n(\vec{r})d\vec{r} \tag{3.11}$$

By summation of (3.10) and (3.11) the inequality

$$E_o^{'} + E_o < E_o + E_o^{'} \tag{3.12}$$

is obtained, which represents an inconsistency. That is to say, there is a one-to-one mapping between the ground state density and the external potential $v(\vec{r})$, although the exact formula is unknown.

3.3.2 Theorem II

It states that the ground state energy can be derived from the electron density by the use of variational calculus. The electron density, which provides a minimum of the ground state energy, is therefore the exact ground state density.

Originally this second theorem has been proved by variation calculus [44], the proof provided subsequently is a different one, namely the so called constrained-search approach, introduced by Levy and Lieb [49, 50] and subsequently thoroughly examined in the books by Parr, Yang as well as Kryachko and Ludena [51, 52].

Since the wave function is a unique functional of the electron density, every trial wave function $\psi^{'}$ corresponds to a trial density $n^{'}(\vec{r})$ following equation (3.2). According to the Rayleigh-Ritz principle, the ground state energy is obtained as

$$E_{v,o} = \min_{\psi^{'}} \langle \psi^{'} | \hat{H} | \psi^{'} \rangle \tag{3.13}$$

In principle, the minimization can be carried out in two steps. In the first step, a trial electron density $n^{'}(\vec{r})$ is fixed. The class of trial functions corresponding to that electron density is then denoted by ${\psi^{'}}^{\alpha}_{n^{'}}$. Then, the constrained energy minimum is defined as

$$E_v[n^{'}(\vec{r})] \equiv \min_{\alpha} \langle {\psi^{'}}^{\alpha}_{n^{'}} | \hat{H} | {\psi^{'}}^{\alpha}_{n^{'}} \rangle = \int v(\vec{r}) n^{'}(\vec{r}) d\vec{r} + F[n^{'}(\vec{r})] \tag{3.14}$$

In that notation, $F[n^{'}(\vec{r})]$ is the universal functional

$$F[n^{'}(\vec{r})] \equiv \min_{\alpha} \langle \psi^{'\alpha}_{n^{'}} | \hat{T} + \hat{U} | \psi^{'\alpha}_{n^{'}} \rangle \tag{3.15}$$

which is clearly related to the Hohenberg-Kohn functional. What is important to notice at this point is that the universal functional $F[n^{'}(\vec{r})]$ requires no explicit knowledge of $v(\vec{r})$.

In the second step, equation (3.14) is minimized over all trial densities $n^{'}(\vec{r})$:

$$E_{v,o} = \min_{n^{'}(\vec{r})} E_v[n^{'}(\vec{r})] = \min_{n^{'}(\vec{r})} \{ \int v(\vec{r}) n^{'}(\vec{r}) d\vec{r} + F[n^{'}(\vec{r})] \} \tag{3.16}$$

Now, for a non-degenerate ground state, the energy in (3.16) is attained, if $n^{'}(\vec{r})$ is the actual ground state density.

3.4 The Kohn-Sham Equations

The framework by Hohenberg and Kohn is exact, yet not very useful in actual calculations. The only possibility would be the direct use of the second Hohenberg-Kohn theorem for energy minimization, a way that is possible in general but has proven itself to be impractical. The most desirable way in which quantities can be calculated for problems without an exact analytical solution is one that allows iterations [34]. An early example of an iterative approach are the self-consistent single particle Hartree-equations [41, 53]. Of course, the Hartree-equations are clearly wave-function based and not directly related to the work of Hohenberg and Kohn, yet they have been proven very useful. Hartree's approximation assumes that every electron moves in an effective single-particle potential of the form

$$v_H(\vec{r}) = -\frac{Z}{|\vec{r}|} + \int \frac{n(\vec{r}^{'})}{|\vec{r} - \vec{r}^{'}|} d\vec{r}^{'} \tag{3.17}$$

The first term is an attractive Coulomb potential of a nucleus with atomic number Z, whereas the integral term corresponds to the potential caused by the mean electron density distribution $n(\vec{r})$

The mean density can be denoted in terms of the single particle wave functions

$$n(\vec{r}) = \sum_{j=1}^{M} |\phi_j(\vec{r})|^2 \tag{3.18}$$

It is important to mention that the sum in (3.18) runs over the M lowest eigenvalues in accordance to the Pauli principle. Since the electron-electron interactions are taken into account in the potential term, the N-electron and therefore (neglecting the spin coordinates) 3N-dimensional Schrödinger equation can be approximately replaced by N 3-dimensional single particle equations for electrons moving in an effective potential defined in (3.17):

$$\left[-\frac{1}{2}\vec{\nabla}^2 + v_H(\vec{r})\right] \phi_j(\vec{r}) = \epsilon_j \phi_j(\vec{r}) \qquad j = 1, \ldots, N \tag{3.19}$$

To solve these self consistent Hartree-equations iteratively an electron density subsequently a potential $v_H(\vec{r})$ are defined, which is then used to solve (3.19) for the chosen wave function. Via comparison of the l.h.s. and the r.h.s. in equation (3.18) one then can determine the deviation of the square-sum of the calculated wave functions from the initially used density. This procedure is repeated with adapted densities in every step until the difference between the l.h.s. and r.h.s. fall behind a certain threshold. Since the framework of Hohenberg and Kohn is formally exact, an extraction of the Hartree equations from their variational principle for the energy should provide even improvements and, more than that, an alternative and finally practically useful formulation of the second theorem [41].

Therefore, Kohn and Sham investigated the density functional theory applied to a system of N non-interacting electrons in an external potential, similar to Hartree's approach. Recalling (3.14) and (3.15), the expression for the energy of such a system is of the form

$$E_{v(\vec{r})}[n^{'}(\vec{r})] \equiv \int v(\vec{r})n^{'}(\vec{r})d\vec{r} + T_S[n^{'}(\vec{r})] \geq E \tag{3.20}$$

where $n^{'}(\vec{r})$ is a v-representable density for non-interacting electrons and $T_S[n^{'}(\vec{r})]$ the kinetic energy of the ground state of those non-interacting electrons [41].

Setup of the Euler-Lagrange equation [54] for the non-interacting case (3.17) with the density defined in (3.19) as argument provides [41]

$$\delta E_v[n^{'}(\vec{r})] \equiv \int \delta n^{'}(\vec{r}) \left[v(\vec{r}) + \frac{\delta}{\delta n^{'}(\vec{r})} T_S[n^{'}(\vec{r})]|_{n^{'}(\vec{r})=n(\vec{r})} - \epsilon \right] d\vec{r} = 0 \tag{3.21}$$

with $n^{'}(\vec{r})$, the exact ground state density for the potential $v(\vec{r})$, and the Lagrangian multiplier ϵ to ensure particle density conservation.

Via equations (3.20) to (3.22), where the approximated Hartree-potential is replaced by a simple external potential, it is possible to calculate the ground state energy and particle density of the non-interacting single particles. For a system of non-interacting electrons, the total ground state energy and particle density can therefore simply be denoted as the sums

$$E = \sum_{j=1}^{N} \epsilon_j \tag{3.22}$$

$$n(\vec{r}) = \sum_{j=1}^{N} |\phi_j(\vec{r})|^2 \tag{3.23}$$

In addition, Kohn and Sham used the universal functional in equations (3.14) to (3.16) as an alternative formulation, namely [41, 55]

$$F[n^{'}(\vec{r})] \equiv T_S[n^{'}(\vec{r})] + \frac{1}{2} \int \frac{[[n^{'}(\vec{r})][n^{'}(\vec{r}^{'})]]}{|\vec{r} - \vec{r}^{'}|} d\vec{r} d\vec{r}^{'} + E_{xc}[n^{'}(\vec{r})] \tag{3.24}$$

In (3.24) $T_S[n'(\vec{r})]$ is the kinetic energy functional of non-interacting electrons (which is not even for the same density $n(\vec{r})$ the true kinetic energy of the interacting system [37]) and the second term is the so-called Hartree term which describes the electrostatic self-repulsion of the electron density [55]. The last term is called exchange-correlation term. It is implicitly defined by (3.24) and can in practice only be approximated. The quality of the the approximation for $E_{xc}[n'(\vec{r})]$ is therefore one of the key issues in DFT [41]. Construction of the Euler-Lagrange equations for the interacting case in equation (3.24) provides [41]

$$\delta E_v[n'(\vec{r})] \equiv \int \delta n'(\vec{r}) \left[v_{eff}(\vec{r}) + \frac{\delta}{\delta n'(\vec{r})} T_S[n'(\vec{r})]|_{n'(\vec{r})=n(\vec{r})} - \epsilon \right] d\vec{r} = 0 \tag{3.25}$$

$$v_{eff}(\vec{r}) \equiv v(\vec{r}) + \int \frac{[n(\vec{r}')]}{|\vec{r} - \vec{r}'|} d\vec{r}' + v_{xc}(\vec{r}) \tag{3.26}$$

and the functional derivative

$$v_{xc}(\vec{r}) \equiv \frac{\delta}{\delta n'(\vec{r})} E_{xc}[n'(\vec{r})]|_{n'(\vec{r})=n(\vec{r})} \tag{3.27}$$

whereas the Euler-Lagrange equation resembles (3.25) up to the potential term. Because of that, the minimizing density can be calculated in a way similar to the Hartree-approach described in equations (3.17) to (3.19). The corresponding equations are the single-particle Schrödinger equations

$$\left[-\frac{1}{2}\vec{\nabla}^2 + v_{eff}(\vec{r}) \right] \phi_j(\vec{r}) = \epsilon_j \phi_j(\vec{r}) \qquad j = 1, 2, \ldots, N \tag{3.28}$$

as well as the defining equation for the particle density

$$n(\vec{r}) = \sum_{j=1}^{M} |\phi_j(\vec{r})|^2 \tag{3.29}$$

which form together with the effective potential $v_{eff}(\vec{r})$ in (3.26) the self-consistent Kohn-Sham equations [41, 55]. The accurate ground state energy, as one of the most important quantities, can be expressed as

$$E = \sum_j \epsilon_j + E_{xc}[n(\vec{r})] - \int v_{xc}(\vec{r}) n(\vec{r}) dv - \frac{1}{2} \int \frac{[n(\vec{r})][n(\vec{r}')]}{|\vec{r} - \vec{r}'|} d\vec{r} d\vec{r}' \tag{3.30}$$

Equation (3.30) can be seen as an generalization of the energy expression obtained with the Hartree-approach (note that the neglect of $E_{xc}[n(\vec{r})]$ and $v_{xc}[n(\vec{r})]$ leads back to equation (3.22) [41]. Similar to the Hohenberg-Kohn theorems, also equations (3.28) to (3.30) are formally exact, which means, if the exact $E_{xc}[n(\vec{r})]$ and $v_{xc}[n(\vec{r})]$ would be used, one would obtain the exact solution.

3.5 The Exchange-Correlation Functionals

3.5.1 Local Density Approximation (LDA)

The simplest approximation to the exchange-correlation functional is the local density approximation (LDA) [56]. The local density approximation is based on the assumption that at every point in the molecule the energy density has the value that would be given by a homogeneous electron gas which had the same electron density r at that point. The energy density is the energy (exchange plus correlation) per electron. Note that the LDA does not assume that the electron density in a molecule is homogeneous (uniform); that drastic situation would be true of a Thomas-Fermi molecule, which, as we said above, cannot exist. The term local was used to contrast the method with ones in which the functional depends not just on r but also on the gradient (first derivative) of r, the contrast apparently arising from the assumption that a derivative is a non-local property. However, under the mathematical definition above a gradient is local, and in fact DFT methods formerly called non-local are now commonly designated as gradient-corrected. LDA functionals have been largely replaced by a family representing an extension of the method, local spin density approximation (LSDA; below) functionals. In fact, in extolling the virtues of a systematic non-empirical ascent of the DFT Jacobs ladder, Perdew et al. slight LDA

and assign to the lowest rung LSDA functionals [57]. As a practical approximate expression for $E_{xc}[n]$, Kohn and Sham suggested what is known in the context of DFT as the local density approximation, or LDA:

$$E_{xc} \simeq \int drn(r)\epsilon_{xc}(n(r)) \tag{3.31}$$

where $\epsilon_{xc}(n)$ is the exchange correlation energy per electron in a uniform electron gas of density n. This quantity is known exactly in the limit of high density, and can be computed accurately at densities of interest, using Monte Carlo techniques (i.e. there are no free parameters). In practice one usually employs parametric formulas, which are fitted to the data and are accurate to within .

Note that the only difference between the resulting computational scheme and a naive mean-field approach is the addition of the potential

$$v_{xc}(r) = \frac{d(n\epsilon_{xc}(n))}{dn}|_n = n(r) \tag{3.32}$$

to the electrostatic potential at the appropriate step in the self-consistency loop. The corresponding expression for the groundstate energy is:

$$E_o = \sum_{i=1}^{N} \epsilon_i - E_{es}[n(r)] + \int drn(r)(\epsilon_{xc}(n(r)) - v_{xc}(n(r)) \tag{3.33}$$

The first term is the non-interacting energy, the second term is half of the Hartree scheme's double counting of the electrostatic energy, and the last term is a similar subtraction for the exchange correlation energy. The LDA has been shown to give very good results for many atomic, molecular and crystalline interacting electron systems, even though in these systems the density of electrons is not slowly varying [58]. The advantage of the homogeneous electron gas model is that it is the only system where the E_{xc} functional is known accurately. In strictly theoretical sense the local approximation is only justified when the density is slowly changing.

However, although the densities in atoms and molecules are typically highly inhomogeneous, LDA still gives surprisingly good results. It has been found, that LDA gives reasonably good results for equilibrium structures, harmonic frequencies and dipole moments in molecules [56].

3.5.2 Generalized-Gradient Approximation (GGA)

As mentioned above, the LDA neglects the inhomogeneities of the real charge density which could be very different from the HEG. The XC energy of inhomogeneous charge density can be significantly different from the HEG result. This leads to the development of various generalized-gradient approximations (GGAs) which include density gradient corrections and higher spatial derivatives of the electron density and give better results than LDA in many cases. Three most widely used GGAs are the forms proposed by Becke (B88), Perdew et al and Perdew, Burke and Enzerhof (PBE). The definition of the XC energy functional of GGA is the generalized form of LSDA to include corrections from density gradient $n(r)$ as

$$E_{XC}^{GGA}[n\uparrow(r), n\downarrow(r)] = \int n(r)\epsilon_X^{hom}(n(r))F_{XC}(n\uparrow(r), n\downarrow(r), |\nabla n\uparrow(r)|, |\nabla n\downarrow(r)|, \ldots)dr \quad (3.34)$$

where ϵ_{XC} is dimensionless and $\epsilon_X^{hom}(n(r))$ is the exchange energy density of the unpolarized HEG. F_{XC} can be decomposed linearly into exchange contribution F_X and correlation contribution F_C as $F_{XC} = F_X + F_C$. For a detailed treatment of F_X and F_C in different GGAs. In general, GGA outperforms LDA in predicting bond length and binding energy of molecules, crystal lattice constants, and other properties, especially in systems with rapidly fluctuating charge density. GGA, on the other hand, has a tendency to overcorrect. The lattice constants from LDA calculations correspond well with experimental data in ionic crystals, however GGA will overestimate it. Nonetheless, in materials where electrons are confined and strongly correlated, such as transition metal oxides and rare-earth elements and compounds, both LDA and GGA function poorly. This flaw causes approximations that go beyond LDA and GGA.

3.5.3 Hybrid Functionals

The idea of hybrid functionals grew out of the attempts to use DFT functionals as a computationally cheap way of correcting Hartree–Fock calculations for correlation effects. Becke formalized the approach [59] in an early hybrid theory that is interesting in itself. Start from the adiabatic connection formula

$$E_{xc} = \int_0^1 U_{xc}^{\lambda} d\lambda \tag{3.35}$$

This integral can be approximated using the mean-value theorem of integration as

$$E_{xc} \approx \frac{1}{2}(U_{xc}^0 + U_{xc}^1) = \frac{1}{2}(E_x + U_{xc}^1) \tag{3.36}$$

where, in the last step, Becke argues [59] that U_{xc}^0 just is E_x. The quantity U_{xc}^1 is the exchange-correlation potential energy of the fully interacting real system. An approximation for the latter can be constructed the same way LDA was constructed,

$$U_{xc}^1 \approx U_{xv}^{LDA} = \int u_{xc}(n(\mathbf{r}))d\mathbf{r} \tag{3.37}$$

The LDA-like functional $u_{xc}(n(\mathbf{r}))$ is derived as an LDA approximation of the potential energy part of the exchange-correlation energy, i.e., $U[n] - J[n]$. Becke obtains [59] an expression to use for u_{xc} from the parametrization of regular LDA correlation by Perdew and Wang [60]. It was later shown [61] how an approximation of U_{xc}^1 can be created from any exchange-correlation functional. For a generic density functional approximation (DFA) one finds

$$U_{xc}^1 \approx U_{xc}^{DFA} = 2E_{xc}^{DFA}[n] - \frac{\partial E_{xc}^{DFA}[n_\gamma]}{\partial \gamma}\Big|_{\gamma=1} \tag{3.38}$$

where n_γ is the scaled density.

Becke's hybrid theory can be viewed both as an correlation correction to the Hartree–Fock scheme, and as a method for incorporating exact exchange into DFT calculations. Becke called it "a true hybrid of its components" and named the two-point adiabatic integration "half-and-half theory".

The half-and-half theory was followed by another three-parameter hybrid formula of Becke [62] that arguably is less connected to formal theory, but was more successful and constitutes the basis for several hybrid functionals in use (e.g., B3LYP [63, 64]),

$$E_{xc} = a_o(E_x - E_x^{LDA}) + E_{xc}^{LDA} + a_x(E_x^{GGA} - E_x^{LDA}) + a_c(E_c^{GGA} - E_c^{LDA}) \quad (3.39)$$

Here a_o, a_x, and a_c are empirical parameters. The use of scaling parameters in the last two terms, which represent the GGA's correction of LDA, was motivated by Becke with the argument that a GGA partly includes a correction of the failure of LDA to produce exact exchange in the $\lambda = 0$ limit. Since the formula manually corrects this problem the GGA's corrections must be scaled down. However, it was remarked by Levy et. Al. [61], that the tree-parameter hybrid formula seems to be a step away from the formal adiabatic connection approach since it apparently drops the λ-derivative in Eq. (3.38). The empirical parameters may be able to correct for this fallacy. Furthermore, Perdew, Ernzerhof and Burke [65] looked at the formula with $a_x = a_c = 1$ and discussed its motivation starting from a simple model for the hybrid coupling-constant dependence:

$$U_{xc}^{\lambda} = E_{xc,\lambda}^{DFA} + (E_x - E_x^{DFA})(1 - \lambda)^{k-1} \quad (3.40)$$

with k an unknown integer. They found that this model led to a theoretical motivation for choosing the value $a_o \approx 0.25$. To implement hybrid functionals in computer code it is quite common to use Hartree–Fock exchange to approximate the exact Kohn–Sham exchange used in the derivation of the Hybrid theory. It is possible that this approximation is somewhat compensated for in the fit of empirical parameters.

Chapter 4

Computational Details

In this thesis, the full potential linearized augmented plane wave (FP-LAPW) method within the DFT implemented in WIEN2k code [66] was employed. To find the optimized ground states of the considered materials, the generalized gradient approximation (GGA) [67] with the Perdew-Burke-Ernzerhof (PBE-GGA) [68] approximation was used. However, since the (PBE-GGA) level of theory underestimates the electronic bandgap [69], to obtain more accurate band gaps the modified Becke and Johanson potential (mBJ) was considered.

The convergence of the basis set was controlled by the cut-off energy -6 Ry. The -6 Ry in WIEN2k specifies the energy below which states are treated as core states. The radii of the muffin-tin for all the calculations are chosen to be 2.5, 2.12, 1.81 and 1.64 a.u for Ca, In, As and O respectively. The cut-off parameter $RK_{max} = 7$ was used, where K_{max} is the plane wave cut-off and R_{MT} is the smallest of all atomic sphere radii. The charge convergence was selected as 0.001 e and energy convergence 0.00001 Ry during self-consistency cycles. Number of k-points in the Brillouin zone was taken 4000 for SCF and 20000 for both DOS and optical properties calculation. E_{max} was set as 3.0 eV for the optical property calculations.

Chapter 5

Results and Discussion

5.1 Structural Properties

The structure of Ca_2InAsO_6 double perovskite compound is generated using the WIEN2k program. This crystal structure is a cubic structure with the space group Fm-3m (space group no: 225).

Table 5.1: Lattice parameters of a unit cell of Ca_2InAsO_6 double perovskite

a ($\mathring{A}$)	**b** ($\mathring{A}$)	**c** ($\mathring{A}$)	**alpha** (α)	**beta** (β)	**gamma** (γ)
7.88003	7.88003	7.88003	90.0000°	90.0000°	90.0000°

The volume of the unit cell is 489.309045 $\mathring{A}^3$. A unit cell of the structure contains 143 atoms, 258 bonds, and 35 polyhedra. Out of the 143 atoms, Ca has 8 atoms, In has 14 atoms, As has 13 atoms, and O has 108 atoms.

The crystal structure of Ca_2InAsO_6 double perovskite is illustrated in **Figure 5.1**.

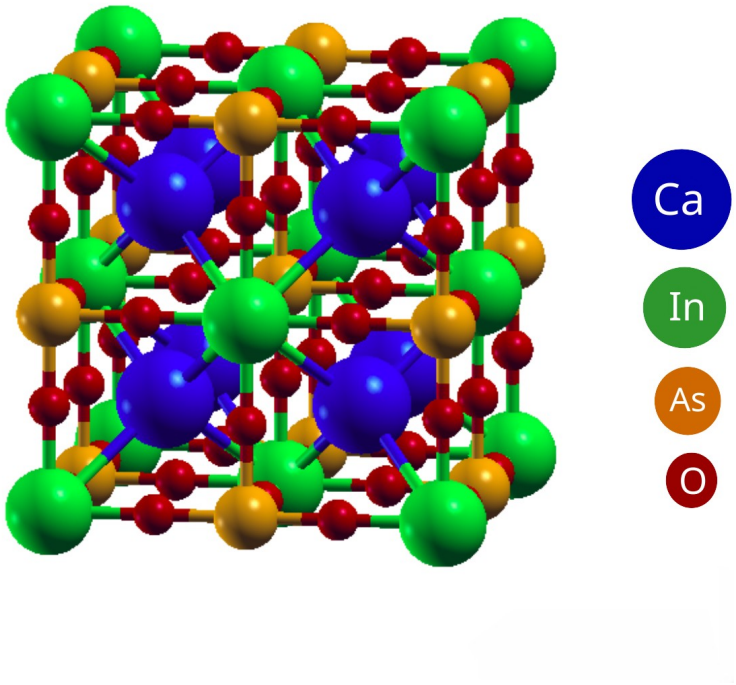

Figure 5.1: Crystal structure of Ca_2InAsO_6 double perovskite

Table 5.2: Wyckoff positions of the constituent atoms of Ca_2InAsO_6 double perovskite

Atom	Number	X	Y	Z
Ca	1	0.75	0.25	0.25
Ca	2	0.25	0.75	0.75
In	1	0	0	0
As	1	0.5	0	0
O	1	0	0.26685750	0
O	2	0	0.73314250	0
O	3	0.73314250	0	0
O	4	0.26685750	0	0
O	5	0	0	0.26685750
O	6	0	0	0.73314250

The crystal formability of a double perovskite oxide $A_2B'B''O_6$ can be evaluated by the tolerance factor (τ) and the octahedral factor (μ) which are defined as follows

$$\tau = \frac{R_A + R_O}{\sqrt{2}\left(\frac{R_{B'}+R_{B''}}{2} + R_O\right)} = \frac{R_A + R_O}{\sqrt{2}\left(\frac{(R_{B'}+R_O)+(R_{B''}+R_O)}{2}\right)} \tag{5.1}$$

$$\mu = \frac{R_{B'} + R_{B''}}{2R_O} \tag{5.2}$$

where R_A, $R_{B'}$, $R_{B''}$ and R_O refer to the ionic radii of A, $B^{'}$, $B^{''}$, O element respectively [70,71]. Statistical studies on the double perovskite structures conducted by Li et al. [72,73], have revealed that for a stable double perovskite $0.71 < \tau < 1.00$ and $0.42 < \mu < 0.75$.

By using the reported ionic radii of Ca ($1\mathring{A}$), In ($0.8\mathring{A}$), As ($0.46\mathring{A}$), O ($1.4\mathring{A}$), the tolerance factor (τ) and the octahedral factor (μ) of about 0.84 and 0.45 are calculated, respectively, confirming that this compound forms a stable structure.

To find the optimized ground state of the considered material, the energy vs volume (E-V) of a unit cell of the crystals were calculated based on the Birch-Murnaghan thermodynamic state relation [74]

$$E(v) = E_o + \frac{9B_oV_o}{16}\left\{\left[\left[\frac{V_o}{V}\right]^{\frac{2}{3}} - 1\right]^3 B_o^{'}\right\} + \frac{9B_oV_o}{16}\left\{\left[\frac{V_o}{V}\right]^{\frac{2}{3}} - 1\right\}^2 + \left\{6 - 4\left[\frac{V_o}{V}\right]^{2/3}\right\} \tag{5.3}$$

In this equation, V_o and V are the ground state unit cell volume and deformed unit cell volume, E_o is the energy of the ground state, B_o is the bulk modulus and $B_o^{'}$ is its derivative. By using this method, the minimum of the E-V curve refers to the ground state of the crystal structure.

From **Figure 5.2**, we found ground state energy -19914.0261 Ry corresponding to ground state unit cell volume 825.456 bohr^3.

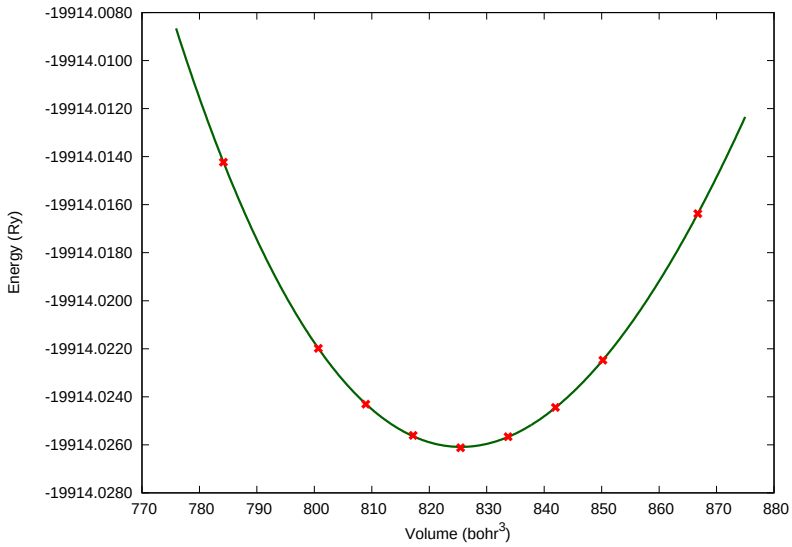

Figure 5.2: Energy vs volume optimization curve for Ca_2InAsO_6 double perovskite

5.2 Band Structure

To find new possible applications of materials, the electronic and optical properties are essential aspects that have to be assessed. To analyze the electronic properties of the considered DP material, we first calculate the band structure with PBE-GGA level of theory. However, as PBE-GGA underestimates the band gap in most cases, to obtain more accurate band gap, we recalculate the electronic property with the modified Becke-Johnson (mBJ) functional [75, 76]. Based on this theory

$$U_{\chi,\sigma}^{mBJ}(r) = CU_{\chi,\sigma}^{BR}(r) + (3C-2)\frac{1}{\pi}\sqrt{\frac{10t_\sigma(r)}{12\rho_\sigma(r)}} \tag{5.4}$$

In this equation, the electron density and the kinetic energy density are given by $\rho_\sigma(r) = \frac{1}{2}\sum_{i=1}^{N_\sigma}|\Psi_{i,\sigma}|^2$, and $t_\sigma(r) = \frac{1}{2}\sum_{i=1}^{N_\sigma}(\nabla\Psi_{i,\sigma}^*)(\nabla\Psi_{i,\sigma})$ respectively and the Becke-Roussel potential is represented by

$$U_{\chi,\sigma}^{BR}(r) = -\frac{1}{b_\sigma(r)}\left(1 - e^{-\chi_\sigma(r)} - \frac{1}{2}\chi_\sigma(r)e^{-\chi_\sigma(r)}\right) \tag{5.5}$$

Here, $\chi_\sigma(r)$ can be calculated by a nonlinear equation which includes $\rho_\sigma(r)$,

$\nabla\rho_\sigma(r)$, $\nabla^2\rho_\sigma(r)$, $t_\sigma(r)$. Moreover, $b_\sigma(r) = [\chi_\sigma^3 e^{-\chi_\sigma/8\pi\rho_\sigma}]$ and

$$C = a + b\left(\frac{1}{V_{unit-cell}}\int_{cell}\frac{\nabla\rho_\sigma(r)}{\rho_\sigma(r)}d^3r'\right)^{1/2} \tag{5.6}$$

In this method, a = -0.012 is a dimensionless parameter, and b = 1.023 bohr$^{1/2}$.

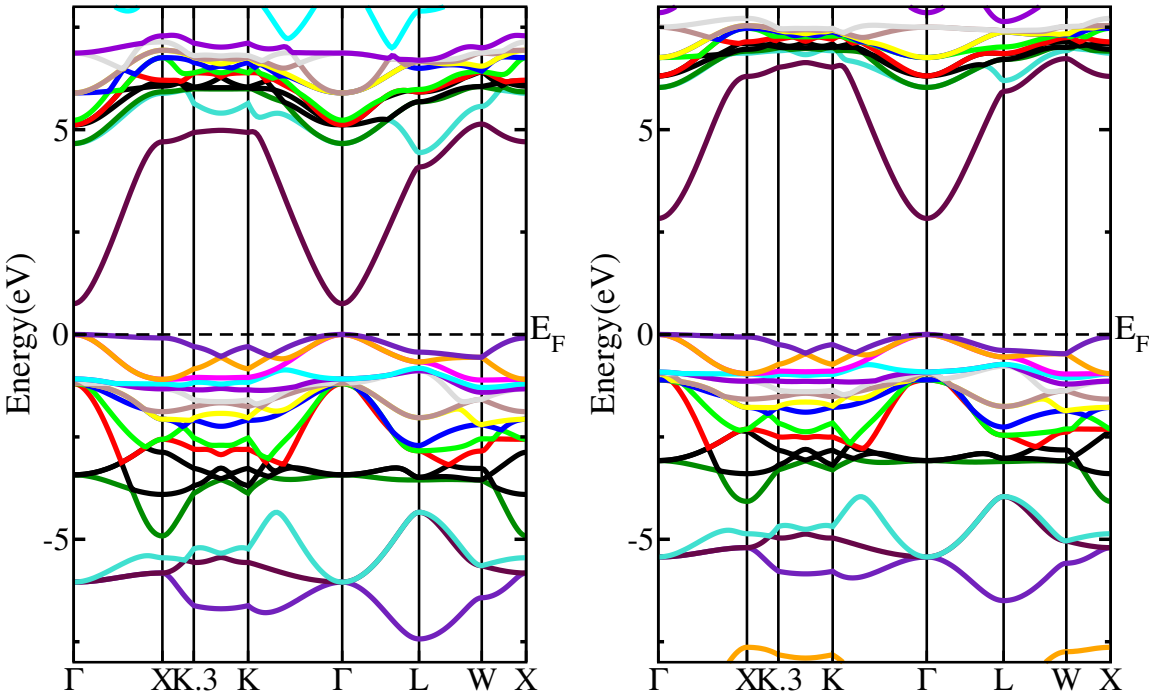

Figure 5.3: The calculated band structure of Ca_2InAsO_6 double perovskite for (a) PBE-GGA and (b) mBJ functionals

Based on our PBE-GGA calculation, Ca_2InAsO_6 is semiconductor with direct band gap of about 0.752 eV. According to our mBJ calculation, the modified direct band gap of about 2.83 eV was estimated for Ca_2InAsO_6 double perovskite. The valence band maximum (VBM) and conduction band minimum (CBM) are located at the Γ point.

5.3 Density of states (DOS)

The number of unique states that electrons can occupy at a given energy level, or the number of electron states per unit volume per unit energy, is known as the density of states (DOS). The bulk properties of conductive substances, such as specific heat, paramagnetic susceptibility, and other transport phenomena, are controlled by this function. The calculated DOS and PDOS for no spin polarization are illustrated, respectively, in **Figure 5.4** and **Figure 5.5**.

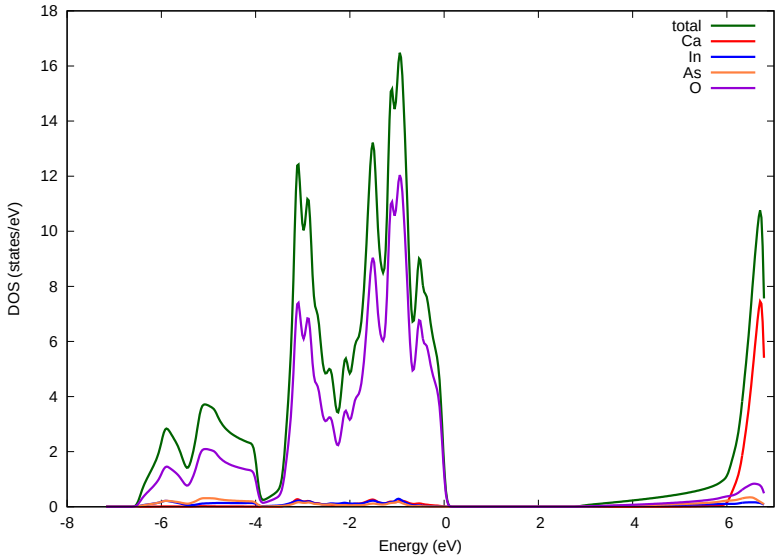

Figure 5.4: Total density of states for Ca_2InAsO_6 double perovskite

For detailed studies of the formation of energy bands, one needs to compute the density of states (DOS) of the system. We got fermi energy for the atoms of 0.4266737240 eV. From **Figure 5.4**, we see that the difference between maximum of valence band and the minimum of conduction band is about 2.83 eV. This band gap is in the range of semiconductor bandgaps. So, it indicates that our compound is a semiconductor. As seen in **Figure 5.4**, total DOS has peaks in the valence band region way more than the conduction band region. It indicates most of the electrons in different atoms aren't free from their respective atoms. We can also say that the contribution of the electrons in O atoms to the valence band is way greater than that of the other atoms. On the other hand, the electrons in Ca atoms contribute more to the conduction band than those in other atoms.

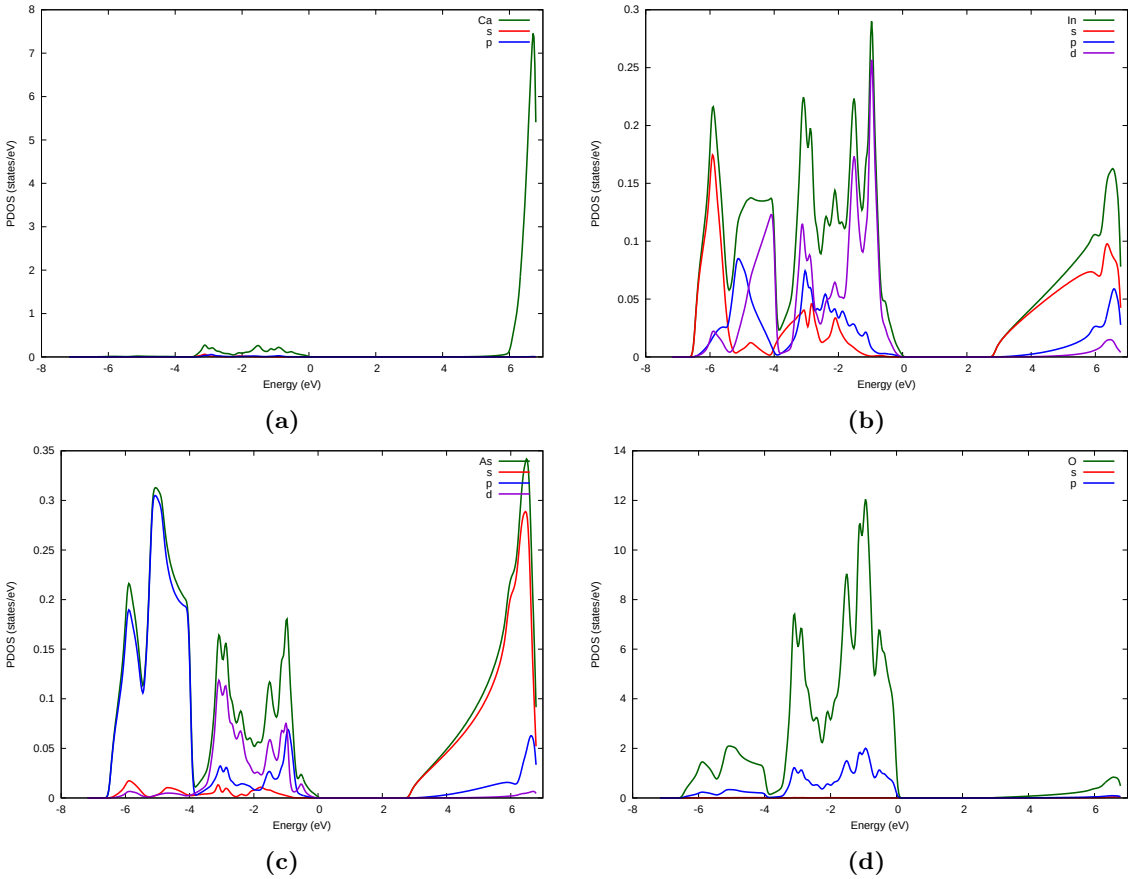

Figure 5.5: Partial density of states of (a) Ca, (b) In, (c) As and (d) O atoms for Ca_2InAsO_6 double perovskite

From **Figure 5.5 (a)**, we can say that the contribution of the electrons of Ca atoms in the conduction band region is more than the valence band region, where the electrons of the s and p orbitals don't contribute significantly. **Figure 5.5 (b)** shows that most of the electrons of the In atom are in the valence band region, and the contribution of the electrons of the d orbital is greater than that of the s and p orbitals. We also see that the sharpest peaks for d and s orbital electrons are near and far from the Fermi energy level, respectively. On the contrary, it is seen that the contribution of s orbital electrons to the conduction band is greater than that of the others following the p orbital. From **Figure 5.5 (c)**, we see that most of the peaks are in the valence band region, but there is also a significant peak in the conduction band region. In the valence band region, p orbital electrons contribute most, followed by d orbital electrons. On the other hand, the contribution of s orbital electrons to the valence band region is way more than the electrons of other orbitals. Now, looking at **Figure 5.5 (d)**, we can say the electrons of O atoms are mostly occupied in the valence band region rather than the conduction band region, and the

electrons of p atoms have a higher concentration than the s ones.

5.4 Optical Properties

5.4.1 Dielectric Function

The frequency-dependent complex dielectric function of the compound can be represented as

$$\varepsilon^*(\omega) = \mathrm{Re}\varepsilon(\omega) + i\,\mathrm{Im}\varepsilon(\omega) \tag{5.7}$$

In which, $\mathrm{Re}\varepsilon(\omega)$ and $\mathrm{Im}\varepsilon(\omega)$ are the real and imaginary components of the function, were calculated. In this formulation, the imaginary component $\mathrm{Im}\varepsilon(\omega)$ is defined as follows [77, 78],

$$\mathrm{Im}\varepsilon^{\alpha\beta}(\omega) = \frac{4\pi^2 e^2}{m^2\omega^2}\sum_{i,f}\int \frac{2d^3k}{(2\pi)^3}\left\{|\langle i_k|P_\alpha^\nu|f_i\rangle|^2 f_i^k(1-f_f^k)\delta(E_f^k - E_i^k - \hbar\omega)\right\} \tag{5.8}$$

i and f introduce the initial and the final state and E_i^k is the corresponding eigenvalue, f_i^k refers to the Fermi distribution and P_α^ν is the projection of the elements of the momentum dipole matrix in the ν direction of the electromagnetic field.

By using $\mathrm{Im}\varepsilon(\omega)$, the real part of the $\varepsilon^*(\omega)$ can be simply obtained by Kramers-Kronig theory [79] as follows:

$$\mathrm{Re}\varepsilon^{\alpha\beta}(\omega) = \delta_{\alpha\beta}\frac{2}{\pi}P_r\int_0^\infty \frac{\mathrm{Im}\varepsilon^{\alpha\beta}(\omega')}{(\omega')^2 - (\omega)^2}d(\omega') \tag{5.9}$$

The light-matter interaction can be described by these two parts of the complex dielectric function. The real part of the dielectric function corresponds to the efficiency of the material to store the field energy and the imaginary component describe the loss of photon energy on the material.

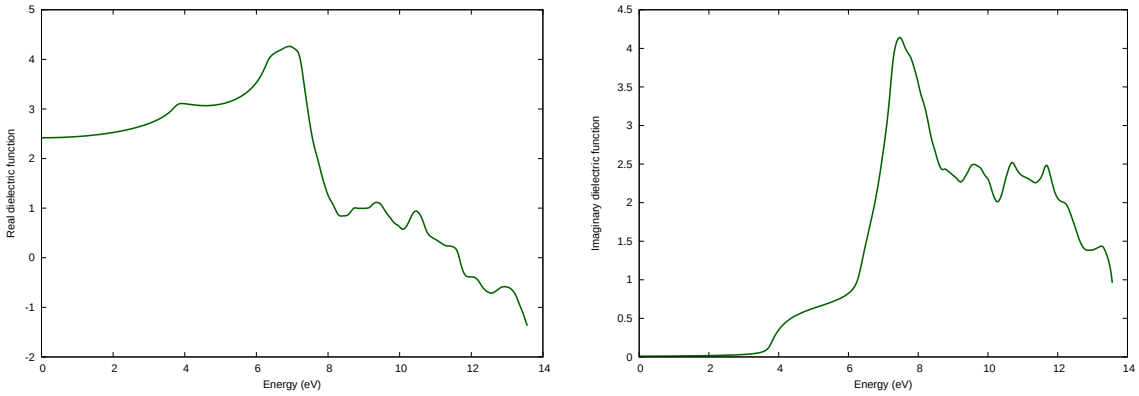

(a) **(b)**

Figure 5.6: (a) Real and (b) Imaginary part of the dielectric function for Ca_2InAsO_6 double perovskite

From **Figure 5.6 (a)** and **Figure 5.6 (b)**, although the most significant peaks for both the real and imaginary components of the function appear in the ultra violet region, this component shows good value in the visible region as well. From **Figure 5.6 (a)**, it is obvious that $\mathrm{Re}\varepsilon(\omega)$ increases with the increasing of the energy and reaches the maximum value of about $\mathrm{Re}\varepsilon(\omega) = 4.26$ at the energy of E = 6.93 eV. For incident photons with an energy of $\hbar\omega > 6.93$ eV, $\mathrm{Re}\varepsilon(\omega)$ decreases with increasing energy. On the other hand, for **Figure 5.6 (b)**, we found that the value of $\mathrm{Im}\varepsilon(\omega)$ is initially zero and remains close to zero in the range from 0.0 eV to 0.42 eV, then increases gradually.

5.4.2 Absorption Coefficient

The absorption coefficient defines how far light of a particular wavelength can penetrate into a material before being absorbed. The absorption coefficient can be written as

$$\alpha(\omega) = \sqrt{2}\left(\sqrt{(\mathrm{Re}\varepsilon(\omega))^2 + (\mathrm{Im}\varepsilon(\omega))^2} - (\mathrm{Re}\varepsilon(\omega))\right)^{\frac{1}{2}} \tag{5.10}$$

If a material has a low absorption coefficient, light will be poorly absorbed. The absorption coefficient depends on both the material and the wavelength of light being absorbed.

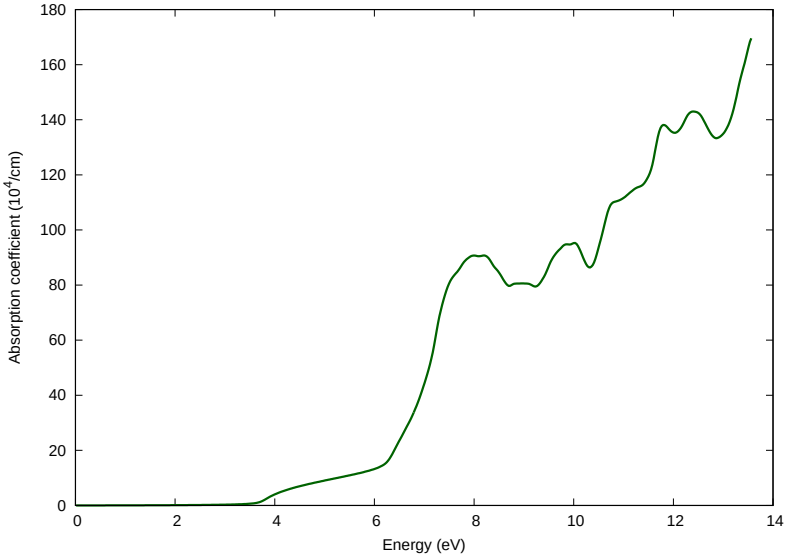

Figure 5.7: The absorption coefficient for Ca_2InAsO_6 double perovskite

From **Figure 5.7**, we can say that although the most significant absorption peaks of the double perovskite appear in the ultra-violet region of the electromagnetic field, this material shows considerable absorption in the visible region of light, which makes it a good candidate for use in electro-optical applications in the visible region.

5.4.3 Refractive Index

The refractive index (n) is an important parameter for the application of optical materials in optics-based devices because of its direct relationship to energy dispersion. The refractive index can be written as

$$n = \frac{1}{\sqrt{2}} \left(\sqrt{(\mathrm{Re}\varepsilon(\omega))^2 + (\mathrm{Im}\varepsilon(\omega))^2} + (\mathrm{Re}\varepsilon(\omega)) \right)^{\frac{1}{2}} \tag{5.11}$$

From **Figure 5.8**, although the most significant peaks appear in the ultra violet region; this component shows good value in the visible region as well. From **Figure 5.8**, it is obvious that the refractive index increases with the increase in energy and reaches its maximum value of about $n = 2.17$ at the energy of E = 7.17 eV. For incident photons with an energy of $\hbar\omega > 7.17$ eV, n decreases with increasing

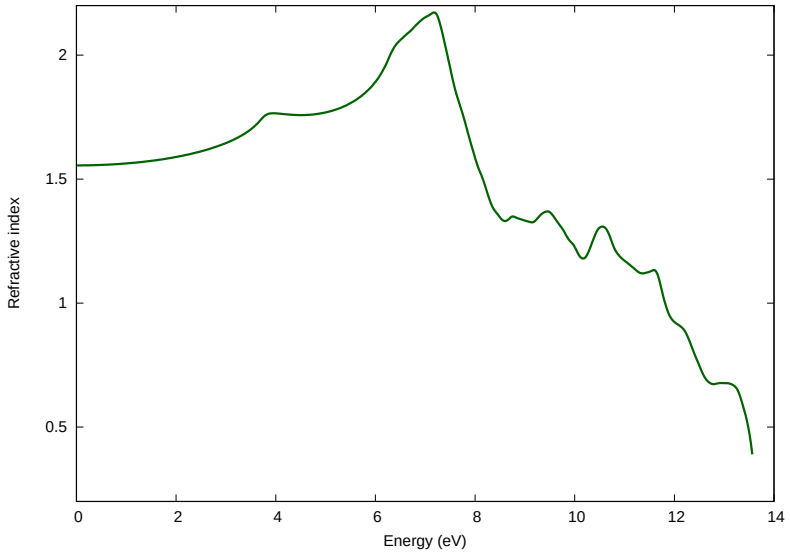

Figure 5.8: The refractive index for Ca_2InAsO_6 double perovskite

energy.

5.4.4 Extinction Coefficient

The absorption and refraction of a medium can be described by a single quantity called the complex refractive index which is written as follows

$$n^* = n + ik \tag{5.12}$$

where the real part n is called the refractive index (n), and the imaginary part k is called the extinction coefficient. The extinction coefficient (k) vanishes for lossless materials. The optical constant k can be written as in terms of the dielectric function $(\mathrm{Re}\varepsilon(\omega), \mathrm{Im}\varepsilon(\omega))$ as

$$k = \frac{1}{\sqrt{2}} \left(\sqrt{(\mathrm{Re}\varepsilon(\omega))^2 + (\mathrm{Im}\varepsilon(\omega))^2} - (\mathrm{Re}\varepsilon(\omega)) \right)^{\frac{1}{2}} \tag{5.13}$$

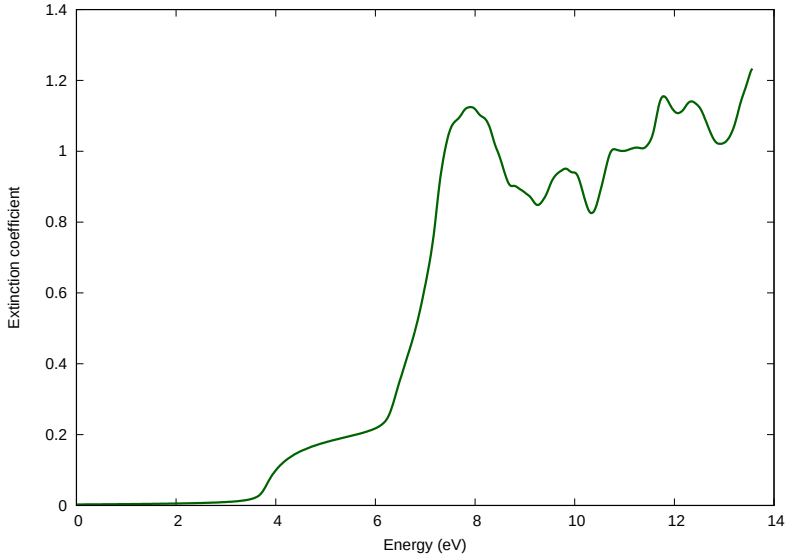

Figure 5.9: The extinction coefficient for Ca_2InAsO_6 double perovskite

From **Figure 5.9**, we can say that although the most significant absorption peaks of the double perovskite appear in the ultra-violet region of the electromagnetic field, this material shows a considerable extinction coefficient in the visible region of light. We found that the value of the extinction coefficient is initially zero and remains close to zero in the range from 0.0 eV to 3.0 eV, then increases gradually.

5.4.5 Optical Conductivity

The optical conductivity is one of the important quantities that describe the optical properties of solids, and it is mainly used to detect any further allowed interband optical transition of a material. The complex optical conductivity ($\sigma^* = \sigma_1 + i\sigma_2$) is related to the real and imaginary parts ($\mathrm{Re}\varepsilon(\omega), \mathrm{Im}\varepsilon(\omega)$) of the complex dielectric function $\varepsilon^*(\omega)$ by the following expressions

$$\sigma_1 = \omega\varepsilon_2\varepsilon_o \tag{5.14}$$

$$\sigma_2 = \omega\varepsilon_1\varepsilon_o \tag{5.15}$$

where ($\omega = 2\pi\nu$) is the angular frequency and ($\varepsilon_o = 8.854 \times 10^{-12}$ Fm^{-1}) is the free space dielectric constant.

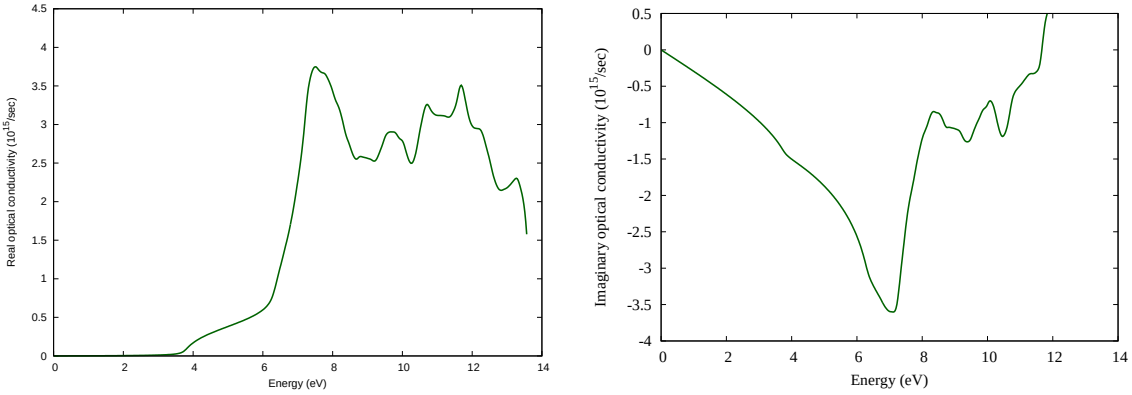

(a) **(b)**

Figure 5.10: (a) Real and (b) Imaginary part of the optical conductivity for Ca_2InAsO_6 double perovskite

From **Figure 5.10 (a)**, we can say that although the most significant peaks of the real part of optical conductivity appear in the ultra-violet region of the electromagnetic field, this material shows a considerable value of σ_1 in the visible region of light. We found that the value of σ_1 is initially zero and remains close to zero in the range from 0.0 eV to 2.87 eV, then increases gradually. From **Figure 5.10 (b)**, we see that at the beginning, the imaginary part of optical conductivity decreases over the increase in energy to a certain point, where the imaginary part of optical conductivity is at its minimum. We found the minimum value to be -3.6 at 7.12 eV. After that minimum value, it increases with increasing energy.

Chapter 6

Conclusions

The structural, electronic, and optical properties of the Ca_2InAsO_6 double perovskite were studied using first-principle calculations on the density functional theory. The tolerance factor (τ) and the octahedral factor (μ) of about 0.84 and 0.45 are calculated, respectively, confirming that this compound forms a stable structure. Our calculations show that Ca_2InAsO_6 is a semiconductor with a moderate Γ point direct bandgap of about 2.83 eV, obtained with the modified Becke-Johnson level of theory. The density of states also revealed the semiconductor nature of this compound. It was observed that the electrons in Oxygen atoms have the most contribution in the valence band region, whereas the electrons in Calcium atoms contribute significantly in the conduction band region. The optical properties show interesting phenomena with good optical absorption in the visible region, which can be effectively tuned by hydrostatic pressure. The structural formability, tunable electronic, and optical properties make it possible to use this compound in different electronic and optical applications.

List of Abbreviations

BZ : Brillouin Zone

CBM : Conduction Band Minimum

DFA : Density Functional Approximation

GGA : Generalized Gradient Approximation

LDA : Local Density Approximation

LEDs : Light-Emitting Diodes

LSDA : Local Spin Density Approximation

mBJ : modified Becke Johnson

PBE : Perdew Burke Ernzerhof

PCE : Power Conversion Efficiency

RHF : Restricted Hatree-Fock

RMT : Radius Muffin Tin

SCF : Self Consistent Field

UHF : Unconstrained Hatree-Fock

VBM : Valence Band Maximum

XC : Exchange Correlation

Bibliography

[1] Zhang, H., Lu, Y., Han, W., Zhu, J., Zhang, Y. and Huang, W., 2020. Solar energy conversion and utilization: Towards the emerging photo-electrochemical devices based on perovskite photovoltaics. Chemical Engineering Journal, 393, p.124766.

[2] Zhou, H., Chen, Q., Li, G., Luo, S., Song, T.B., Duan, H.S., Hong, Z., You, J., Liu, Y. and Yang, Y., 2014. Interface engineering of highly efficient perovskite solar cells. Science, 345(6196), pp.542-546.

[3] Burschka, J., Pellet, N., Moon, S.J., Humphry-Baker, R., Gao, P., Nazeeruddin, M.K. and Grätzel, M., 2013. Sequential deposition as a route to high-performance perovskite-sensitized solar cells. Nature, 499(7458), pp.316-319.

[4] Wong, A.B., Lai, M., Eaton, S.W., Yu, Y., Lin, E., Dou, L., Fu, A. and Yang, P., 2015. Growth and anion exchange conversion of CH3NH3PbX3 nanorod arrays for light-emitting diodes. Nano letters, 15(8), pp.5519-5524.

[5] Zheng, E., Yuh, B., Tosado, G.A. and Yu, Q., 2017. Solution-processed visible-blind UV-A photodetectors based on CH 3 NH 3 PbCl 3 perovskite thin films. Journal of Materials Chemistry C, 5(15), pp.3796-3806.

[6] Eames, C., Frost, J.M., Barnes, P.R., O'regan, B.C., Walsh, A. and Islam, M.S., 2015. Ionic transport in hybrid lead iodide perovskite solar cells. Nature communications, 6(1), p.7497.

[7] Roknuzzaman, M., Ostrikov, K.K., Wasalathilake, K.C., Yan, C., Wang, H. and Tesfamichael, T., 2018. Insight into lead-free organic-inorganic hybrid perovskites for photovoltaics and optoelectronics: A first-principles study. Organic Electronics, 59, pp.99-106.

[8] Shahbazi, M. and Wang, H., 2016. Progress in research on the stability of organometal perovskite solar cells. Solar Energy, 123, pp.74-87.

[9] Brik, M.G., 2012. First-principles calculations of electronic, optical and elastic properties of Ba2MgWO6 double perovskite. Journal of Physics and Chemistry of Solids, 73(2), pp.252-256.

[10] Khandy, S.A. and Gupta, D.C., 2020. Magneto-electronic, mechanical, thermoelectric and thermodynamic properties of ductile perovskite Ba2SmNbO6. Materials Chemistry and Physics, 239, p.121983.

[11] Saxena, M. and Maiti, T., 2017. Effect of Ba-doping on high temperature thermoelectric properties of Sr2TiMoO6 double perovskites. Journal of Alloys and Compounds, 710, pp.472-478.

[12] Rai, D.P., Shankar, A., Ghimire, M.P. and Thapa, R.K., 2015. The electronic, magnetic and optical properties of double perovskite A2FeReO6 (A= Sr, Ba) from first principles approach. Computational Materials Science, 101, pp.313-320.

[13] Saxena, M., Tanwar, K. and Maiti, T., 2017. Environmental friendly Sr2TiMoO6 double perovskite for high temperature thermoelectric applications. Scripta Materialia, 130, pp.205-209.

[14] Majid, A., Khan, A. and Choi, T.S., 2011. Predicting lattice constant of complex cubic perovskites using computational intelligence. Computational Materials Science, 50(6), pp.1879-1888.

[15] Ullah, R., Ali, M.A., Haq, B.U., Khan, A., Mahmood, Q. and Murtaza, G., 2022. Exploring electronic, structural, magnetic and thermoelectric properties of novel Ba2EuMoO6 double perovskite. Materials Science in Semiconductor Processing, 137, p.106218.

[16] Murtaza, G., Alshahrani, T., Khalil, R.A., Mahmood, Q., Flemban, T.H., Althib, H. and Laref, A., 2021. Lead free double perovsites halides X2AgTlCl6 (X= Rb, Cs) for solar cells and renewable energy applications. Journal of Solid State Chemistry, 297, p.121988.

[17] Hassan, M., Shahid, A. and Mahmood, Q.J.S.S.C., 2018. Structural, electronic, optical and thermoelectric investigations of antiperovskites A3SnO

(A= Ca, Sr, Ba) using density functional theory. Solid State Communications, 270, pp.92-98.

[18] Noor, N.A., Mahmood, Q., Rashid, M., Haq, B.U. and Laref, A., 2018. The pressure-induced mechanical and optoelectronic behavior of cubic perovskite PbSnO3 via ab-initio investigations. Ceramics International, 44(12), pp.13750-13756.

[19] Yue, L., Yan, B., Attridge, M. and Wang, Z., 2016. Light absorption in perovskite solar cell: Fundamentals and plasmonic enhancement of infrared band absorption. Solar Energy, 124, pp.143-152.

[20] AlObaid, A.A., Rouf, S.A., Al-Muhimeed, T.I., Aljameel, A.I., Bouzgarrou, S., Hegazy, H.H., Alshahrani, T., Nazir, G., Mera, A. and Mahmood, Q., 2021. New lead-free double perovskites (Rb2GeCl/Br) 6; a promising materials for renewable energy applications. Materials Chemistry and Physics, 271, p.124876.

[21] Tian, Y., Xu, B. and Zhao, Z., 2012. Covalent-bonded graphene polymers with high hardness. Int. J. Refract. Metals Hard Mater., 33, pp.93-106.

[22] Xin, B., Pak, Y., Mitra, S., Almalawi, D., Alwadai, N., Zhang, Y. and Roqan, I.S., 2019. Self-patterned CsPbBr3 nanocrystals for high-performance optoelectronics. ACS applied materials interfaces, 11(5), pp.5223-5231.

[23] Bakr, O.M. and Mohammed, O.F., 2017. Powering up perovskite photoresponse. Science, 355(6331), pp.1260-1261.

[24] Yang, Y. and You, J., 2017. Make perovskite solar cells stable. Nature, 544(7649), pp.155-156.

[25] Yin, W.J., Shi, T. and Yan, Y., 2014. Unique properties of halide perovskites as possible origins of the superior solar cell performance. Advanced materials, 26(27), pp.4653-4658.

[26] Kovalenko, M.V., Protesescu, L. and Bodnarchuk, M.I., 2017. Properties and potential optoelectronic applications of lead halide perovskite nanocrystals. Science, 358(6364), pp.745-750.

[27] Chen, J., Zhou, S., Jin, S., Li, H. and Zhai, T., 2016. Crystal organometal halide perovskites with promising optoelectronic applications. Journal of Materials Chemistry C, 4(1), pp.11-27.

[28] Roknuzzaman, M., Ostrikov, K., Wang, H., Du, A. and Tesfamichael, T., 2017. Towards lead-free perovskite photovoltaics and optoelectronics by ab-initio simulations. Scientific reports, 7(1), p.14025.

[29] Parr, R.G. and Yang, W., 1980. Horizons of quantum chemistry. Horizons of Quantum Chemistry. Springer. https://doi. org/10.1007/978-94-009-9027-2.

[30] Schrödinger, E., 1926. An undulatory theory of the mechanics of atoms and molecules. Physical review, 28(6), p.1049.

[31] Schwabl, F., 2007. Quantum mechanics (QM I). ; Quantenmechanik (QM I). Eine Einfuehrung.

[32] Rajaniemi, T., 2016. Electronic and optical properties of TiO nanoclusters (Master's thesis, T. Rajaniemi).

[33] Young, D.C., 2001. A practical guide for applying techniques to real-world problems. Computational Chemistry, New York, 9, p.390.

[34] Capelle, K., 2006. A bird's-eye view of density-functional theory. Brazilian journal of physics, 36, pp.1318-1343.

[35] Parts, M.Q.M., 1977. I and II: An Introduction to Quantum Chemistry (Volume 1), PW Atkins.

[36] Szabo, A. and Ostlund, N.S., 2012. Modern quantum chemistry: introduction to advanced electronic structure theory. Courier Corporation.

[37] Koch, W. and Holthausen, M.C., 2015. A chemist's guide to density functional theory. John Wiley Sons.

[38] Griffiths, D.J. and Schroeter, D.F., 2018. Introduction to quantum mechanics. Cambridge university press.

[39] Dirac, P.A.M., 1939, July. A new notation for quantum mechanics. In Mathematical Proceedings of the Cambridge Philosophical Society (Vol. 35, No. 3, pp. 416-418). Cambridge University Press.

[40] Lang, C.B., Pucker, N., Lang, C.B. and Pucker, N., 2016. Elemente der Tensorrechnung. Mathematische Methoden in der Physik, pp.411-440.

[41] Kohn, W., 1999. Nobel Lecture: Electronic structure of matter—wave functions and density functionals. Reviews of Modern Physics, 71(5), p.1253.

[42] Löwdin, P.O., 1959. Scaling problem, virial theorem, and connected relations in quantum mechanics. Journal of Molecular Spectroscopy, 3(1-6), pp.46-66.

[43] Josefsson, I., Kunnus, K., Schreck, S., Föhlisch, A., de Groot, F., Wernet, P. and Odelius, M., 2012. Ab initio calculations of x-ray spectra: Atomic multiplet and molecular orbital effects in a multiconfigurational scf approach to the l-edge spectra of transition metal complexes. The journal of physical chemistry letters, 3(23), pp.3565-3570.

[44] Hohenberg, P. and Kohn, W., 1964. Inhomogeneous Electron Gas. Physi-cal Review, 136, B864.

[45] Thomas, L.H., 1927, January. The calculation of atomic fields. In Mathematical proceedings of the Cambridge philosophical society (Vol. 23, No. 5, pp. 542-548). Cambridge University Press.

[46] Fermi, E., 1927. Un metodo statistico per la determinazione di alcune priorieta dell'atome. Rend. Accad. Naz. Lincei, 6(602-607), p.32.

[47] Fermi, E., 1928. Eine statistische Methode zur Bestimmung einiger Eigenschaften des Atoms und ihre Anwendung auf die Theorie des periodischen Systems der Elemente. Zeitschrift für Physik, 48(1-2), pp.73-79.

[48] Fermi, E., 1928. Sulla deduzione statistica di alcune proprietá dell'atomo. Applicazione alla teoria del sistema periodico degli elementi. Rend. Lincei, 7, p.342.

[49] Levy, M., 1979. Universal variational functionals of electron densities, first-order density matrices, and natural spin-orbitals and solution of the v-representability problem. Proceedings of the National Academy of Sciences, 76(12), pp.6062-6065.

[50] Lieb, E.H., 2002. Density functionals for Coulomb systems. Inequalities: Selecta of Elliott H. Lieb, pp.269-303.

[51] Parr, R.G. and Yang, W., 1989. Density-functional theory of atoms and molecules Oxford Univ. Press, New York.

[52] E.V. Kryachko, E.S. Ludena. Systems . Energy Density Functional Theory of Many- Electron Kluwer Academic Press, 1990.

[53] Riane Khaula SOUDANI, Z.L., Étude théorique de N, O-nucléosides par réaction 1, 3-dipolaire (1, 3-DC).

[54] TORSTEN. FLIESSBACH, 2020. MECHANIK: lehrbuch zur theoretischen physik. SPRINGER.

[55] Kohn, W. and Sham, L.J., 1965. Self-consistent equations including exchange and correlation effects. Physical review, 140(4A), p.A1133.

[56] Rajaniemi, T., 2016. Electronic and optical properties of TiO nanoclusters (Master's thesis, T. Rajaniemi).

[57] Lewars, E.G., 2011. Computational chemistry. Introduction to the theory and applications of molecular and quantum mechanics, 318.

[58] Argaman, N. and Makov, G., 1998. Density Functional Theory: a brief introduction (No. physics/9806013).

[59] Becke, A.D., 1993. A new mixing of Hartree–Fock and local density-functional theories. The Journal of chemical physics, 98(2), pp.1372-1377.

[60] Perdew, J.P. and Wang, Y., 2018. Erratum: Accurate and simple analytic representation of the electron-gas correlation energy [Phys. Rev. B 45, 13244 (1992)]. Physical Review B, 98(7), p.079904.

[61] Levy, M., March, N.H. and Handy, N.C., 1996. On the adiabatic connection method, and scaling of electron–electron interactions in the Thomas–Fermi limit. The Journal of chemical physics, 104(5), pp.1989-1992.

[62] Raghavachari, K., 2000. Perspective on "Density functional thermochemistry. III. The role of exact exchange" Becke AD (1993) J Chem Phys 98: 5648–52. Theoretical Chemistry Accounts, 103, pp.361-363.

[63] Stephens, P.J., Devlin, F.J., Chabalowski, C.F. and Frisch, M.J., 1994. Ab initio calculation of vibrational absorption and circular dichroism spectra using density functional force fields. The Journal of physical chemistry, 98(45), pp.11623-11627.

[64] Hertwig, R.H. and Koch, W., 1997. On the parameterization of the local correlation functional. What is Becke-3-LYP?. Chemical Physics Letters, 268(5-6), pp.345-351.

[65] Perdew, J.P., Ernzerhof, M. and Burke, K., 1996. Rationale for mixing exact exchange with density functional approximations. The Journal of chemical physics, 105(22), pp.9982-9985.

[66] Grimme, S., 2006. Semiempirical GGA-type density functional constructed with a long-range dispersion correction. Journal of computational chemistry, 27(15), pp.1787-1799.

[67] Perdew, J.P., Burke, K. and Ernzerhof, M., 1996. Generalized gradient approximation made simple. Physical review letters, 77(18), p.3865.

[68] Berber, M., Bouzouira, N., Mebrek, M., Boudali, A., Abid, H. and Moujri, H., 2020. Structural, electronic, and optical properties of quaternary alloys Al0. 50Ga0. 50NxSb1-x: a first-principles study. Revista mexicana de física, 66(6), pp.790-796.

[69] Koller, D., Tran, F. and Blaha, P., 2011. Merits and limits of the modified Becke-Johnson exchange potential. Physical Review B, 83(19), p.195134.

[70] Cai, Y., Xie, W., Teng, Y.T., Harikesh, P.C., Ghosh, B., Huck, P., Persson, K.A., Mathews, N., Mhaisalkar, S.G., Sherburne, M. and Asta, M., 2019. High-throughput computational study of halide double perovskite inorganic compounds. Chemistry of Materials, 31(15), pp.5392-5401.

[71] Meyer, E., Mutukwa, D., Zingwe, N. and Taziwa, R., 2018. Lead-free halide double perovskites: a review of the structural, optical, and stability properties as well as their viability to replace lead halide perovskites. Metals, 8(9), p.667.

[72] Li, C., Soh, K.C.K. and Wu, P., 2004. Formability of ABO3 perovskites. Journal of alloys and compounds, 372(1-2), pp.40-48.

[73] Li, C., Lu, X., Ding, W., Feng, L., Gao, Y. and Guo, Z., 2008. Formability of abx3 (x= f, cl, br, i) halide perovskites. Acta Crystallographica Section B: Structural Science, 64(6), pp.702-707.

[74] Birch, F., 1978. Finite strain isotherm and velocities for single-crystal and polycrystalline NaCl at high pressures and 300 K. Journal of Geophysical Research: Solid Earth, 83(B3), pp.1257-1268.

[75] Koller, D., Tran, F. and Blaha, P., 2011. Merits and limits of the modified Becke-Johnson exchange potential. Physical Review B, 83(19), p.195134.

[76] Monkhorst, H.J. and Pack, J.D., 1976. Special points for Brillouin-zone integrations. Physical review B, 13(12), p.5188.

[77] Wooten, F., 1972. Optical properties of solids. Academic Press.

[78] Bakhtiar, U.H., Ahmed, R., Khenata, R., Ahmed, M. and Hussain, R., 2013. A first-principles comparative study of exchange and correlation potentials for ZnO. Materials science in semiconductor processing, 16(4), pp.1162-1169.

[79] Babaei, M., Ahmadi, V. and Darvish, G., 2022. Opto-electro-mechanical properties of lead-free hybrid double perovskites Cs2AgSbX6 (X= Cl, Br, I) for solar cells: A first-principles study. Journal of Physics and Chemistry of Solids, 169, p.110880.